

Drell-Yan Measurements of Nucleon and Nuclear Structure with the FNAL Main Injector

Funding Proposal
submitted to
The United States Department of Energy

L. D. Isenhower, M. E. Sadler, R. S. Towell
Abilene Christian University, Abilene, TX 79699

J. Arrington, D. F. Geesaman (Co-Spokesperson), R. J. Holt, H. E. Jackson,
P. E. Reimer (Co-Spokesperson), D. H. Potterveld
Argonne National Laboratory, Argonne IL 60439

C. N. Brown
Fermi National Accelerator Laboratory, Batavia, IL 60510

G. T. Garvey, M. J. Leitch, P. L. McGaughey
Los Alamos National Laboratory, Los Alamos, NM 87545

R. Gilman, C. Glashauser, X. Jiang, R. Ransome, S. Strauch
Rutgers University, Rutgers, NJ 08544

C. A. Gagliardi, R. E. Tribble, M. A. Vasiliev
Texas A & M University, College Station, TX 77843-3366

E. Kinney
University of Colorado, Boulder, CO 80309-0390

J.-C. Peng
University of Illinois, Urbana, IL 61081

D. D. Koetke
Valparaiso University, Valparaiso, IN 46383

(The P906 Collaboration)

November 14, 2002

Summary:

Drell-Yan Measurements of Nucleon and Nuclear Structure with the FNAL Main Injector

An experiment to measure nucleon and nuclear structure at the parton level using Drell-Yan scattering is presented. This experiment will use the 120 GeV proton beam extracted from the Fermilab Main Injector. The experiment (designated E906) has been approved by the Fermilab PAC, and requires funds for the construction of a large focusing dipole magnet (approximately \$1.96M) and modest additional detector funds (approximately \$720k).

In the Drell-Yan process, a quark (antiquark) in the beam hadron annihilates with an antiquark (quark) in the target. In the limit of large x -Feynman, only the beam quark and target antiquark terms are important; hence, Drell-Yan scattering may be used probe the antiquark sea of the target hadron. It may also be used to measure the the interactions of the initial state quark in the nuclear medium. Several previous Drell-Yan experiments have already exploited these properties, but these experiments were limited by statistics to rather low values of parton fractional momentum, x . At fixed x , the Drell-Yan cross section scales as the inverse of the square of the center-of-mass energy. Because of this, at the lower beam energy of the Fermilab Main Injector, the Drell-Yan cross section is a factor of seven *higher* than in previous Fermilab Tevatron (800 GeV beam) Drell-Yan experiments. At the same time, most backgrounds (primarily J/ψ production) scale with the square of the center-of-mass energy. As such, they will be suppressed in a Main Injector experiment. The Fermilab E906 collaboration will exploit this to make several important physics measurements at larger values of x than previously achievable.

While perturbative Quantum Chromodynamics (QCD) provides a good description of the evolution of the proton's parton distributions, it provides no clues as to their origins. With Drell-Yan's sensitivity to the antiquark distributions, it can be used to measure the ratio of anti-down to anti-up, \bar{d}/\bar{u} , quarks in the proton. As measured in previous Drell-Yan experiments, this ratio is far from unity for moderate values of x —indicating a significant non-perturbative component in the proton's sea. At larger values of x , the data appear to show that the strengths of the \bar{d} and \bar{u} distributions becoming more equal, possibly indicating that the perturbatively generated sea is becoming dominant again. Fermilab E906 will have the reach to study this region and conclusively determine the ratio of \bar{d}/\bar{u} from measurements on liquid hydrogen and deuterium targets.

As $x \rightarrow 1$, there is considerable uncertainty in the distributions of valence quarks. In part, this is due to a lack of proton data, and in part, due to uncertainties in nuclear corrections, which are significant as $x \rightarrow 1$, even in deuterium. The absolute Drell-Yan cross section is sensitive to these high- x parton distributions in the *beam proton*. Data from previous Drell-Yan experiment shows a discrepancy with next-to-leading order cross section calculations which could be attributed to the uncertainty in the ratio d_v/u_v as $x \rightarrow 1$. The proton-proton absolute cross section measurements from Fermilab E906 will provide the data—free of nuclear corrections—needed to determine the behavior of $4u + d$ as $x \rightarrow 1$.

When the proton is contained in a nucleus, the proton's parton distributions appear to be modified. In addition to hydrogen and deuterium, data will be collected on a variety of nuclear targets to study these changes. Pions in meson exchange models of nuclear binding should lead to an enhancement of the antiquark sea in nuclei when compared to deuterium. While this was not seen by previous Drell-Yan experiments, the large statistical uncertainty at high x allowed considerable freedom for these models. Due to the increased cross section at higher x Fermilab E906 will be able to significantly constrain these models. Absolute cross section measurements on deuterium will provide a measurement of $\bar{d}(x) + \bar{u}(x)$, a quantity so far only accessible through

neutrino deep inelastic scattering cross section measurements on heavy nuclear targets. At the same time, the absolute cross section measurements on nuclear targets will determine how nuclear effects might influence the interpretation of the neutrino results.

Finally, the Drell-Yan process can be used to study the interactions of fast, colored partons traversing cold nuclei. Since the final state particles, muons, only interact electromagnetically and not strongly, only the initial state strong interactions of the incident quarks are apparent. This makes Drell-Yan an ideal laboratory to study the energy loss of partons in nuclei—a subject of considerable interest to the Relativistic Heavy Ion community. Several models have been proposed to describe the energy loss process. With these models by comparing different nuclei, previous Drell-Yan experiments have placed limits on parton energy loss. Because of an increased sensitivity to energy loss at lower beam energy and higher statistics, this experiment will be able to measure this energy loss and quantitatively distinguish between competing models.

The apparatus to be constructed is very similar to that used by previous high-rate 800 GeV Drell-Yan experiments at Fermilab. In fact it will reuse many of the detector components and much of the electronics from these and other Fermilab experiments. The proposed apparatus consists of two large dipole magnets and a number of tracking/triggering stations. The liquid hydrogen, liquid deuterium and solid atomic targets are positioned up stream of the first magnet. The first magnet, which focuses the muons produced in the target, will contain the beam dump and a thick wall of absorber material, designed to allow only muons to traverse the active detector elements. The second magnet provided the primary momentum measurement of the muons. Between the two magnets and after the second magnet will be a total of four tracking and triggering stations. Because of the lower beam energy, relative to previous Drell-Yan experiments, the entire layout of the experiment must be contracted along the beam axis. This necessitates the construction of a new muon focusing magnet. The new magnet will be roughly one third as long as the magnet used by the previous Fermilab Drell-Yan experiments. Fortunately, the iron from the old magnet is available and can be reused in the new magnet; however, new coils will need to be constructed. This represents the bulk of the equipment funds requested here. The remainder of the funds will be used to replace aging equipment from the previous experiment and to upgrade the trigger system to handle the de-bunched beam and enhance the trigger-level track finding.

In order to finish construction of the apparatus in a timely manner, funding must begin in FY2005 with roughly \$600k for magnet design work and prototyping of custom trigger electronics. In FY2006, the bulk of the magnet construction will take place, requiring \$1.56M. In FY2007, the magnet construction will be finished and detectors will be installed, requiring \$516k.

Contents

| | |
|---|-----------|
| Summary | i |
| 1 Introduction | 1 |
| 2 Discussion of Physics | 3 |
| 2.1 Parton Distributions: $\bar{d}(x)/\bar{u}(x)$ of the Proton | 4 |
| 2.1.1 Origins of the Nucleon Sea | 5 |
| 2.1.2 Interpretability of the Results: QCD factorization | 7 |
| 2.1.3 Competing Measurements of \bar{d}/\bar{u} | 7 |
| 2.2 Measurements of Other Parton Distributions | 9 |
| 2.3 Antiquark Distributions of Nuclei | 9 |
| 2.4 Partonic Energy Loss | 11 |
| 2.5 Possible Future Measurements | 16 |
| 3 Experimental Apparatus | 16 |
| 3.1 Beam and Targets | 18 |
| 3.2 Magnets | 18 |
| 3.3 Tracking Chambers | 20 |
| 3.4 Scintillator Hodoscopes | 21 |
| 3.5 Muon Identification | 22 |
| 3.6 Trigger | 22 |
| 3.7 Monte Carlo of Trigger and Spectrometer Rates | 24 |
| 3.8 Data Acquisition System | 26 |
| 3.9 Analysis | 28 |
| 3.10 Yields | 29 |
| 4 Costs and Schedule | 29 |
| 5 Collaboration | 35 |
| 6 Facilities and Resources | 36 |
| 7 Conclusions | 36 |

1 Introduction

While proton structure functions have been measured with deep inelastic scattering over five orders of magnitude in both the fractional momentum of the parton, x , and the virtuality of the incident photon, Q^2 , the factorizable, non-perturbative parton distributions must be determined by phenomenological fits [1, 2, 3, 4, 5, 6]. Perturbative Quantum Chromodynamics (QCD) quantitatively describes the Q^2 evolution of the parton distributions, but the origins of the parton distributions themselves have not proved amenable to QCD treatment, although many *models* exist in the literature. Measurements of those distributions that are poorly determined provide vital information on nucleon structure which is used to constrain and refine the phenomenology.

Each time new data have tested underlying assumptions of the phenomenology, the phenomenology has been found wanting. For example, no known symmetry requires the equality of the anti-down [$\bar{d}_p(x)$] and anti-up [$\bar{u}_p(x)$]¹ quark distributions in the proton, but until 1991, this was a common assumption. The first evidence to the contrary was the NMC observation [7] that the integral of $\bar{d}(x) - \bar{u}(x)$ is non-zero. NA51 [8] used the Drell-Yan process to confirm the non-equality of $\bar{d}(x)$ and $\bar{u}(x)$. Fermilab E866/NuSea [9, 10, 11] recently measured the x dependence of $\bar{d}(x)/\bar{u}(x)$ and $\bar{d}(x) - \bar{u}(x)$ from $0.015 < x < 0.35$. When these data were included in the CTEQ5 [2] and MRST [5] global fits, both the sea and valence distributions differ substantially from previous parameterizations, as shown in Fig. 1. Fermilab E866 observed a striking asymmetry in the sea distributions at moderate x ; however, as x increases, the sea appears to be becoming more flavor symmetric—a sign of a possible change in the mechanism generating the sea. At the same time, however, the statistical uncertainty of the data grows significantly.

In order to answer a number of interesting questions relating to the parton structure of nuclei and the nucleus at higher x , including the uncertainty in the $\bar{d}(x)/\bar{u}(x)$ ratio, the Fermilab E906 collaboration plans to make precise measurements of proton-induced Drell-Yan cross sections on hydrogen, deuterium and heavy nuclear targets using the Fermilab Main Injector as a proton source. The lower beam energy of the Main Injector (120 GeV/c) provides an excellent opportunity to study these distributions at larger x . For fixed x , the Drell-Yan cross section is inversely proportional to the square of the center-of-mass energy, s . At the same time, the primary background, J/ψ production, which scales with s , is reduced, allowing a more intense proton beam to be used. The combination of these yield a factor of 50 increase in Drell-Yan events for the same amount of beam time. From these measurements the ratio $\bar{d}(x)/\bar{u}(x)$ for $0.1 < x < 0.45$ will be determined.

The results of these measurements will also have implications in other areas. For example, in proton-proton collider experiments the highest energy scales are achieved via $q\bar{q}$ annihilation of large x partons. The ratio of $\bar{d}(x)/\bar{u}(x)$ results from a competition between non-perturbative and QCD gluon splitting contributions and high x results may provide constraints on the gluon distributions at high x that evolve into the antiquark distributions needed at high mass scales.

The absolute Drell-Yan cross sections on hydrogen and deuterium are also of great interest. In the proton, as $x \rightarrow 1$ there is considerable freedom in the $d(x)/u(x)$ *quark* distribution. Through the *beam* parton distributions, the Drell-Yan cross section probes the linear combination $4u(x) + d(x)$. The uncertainty in the parton distributions at high- x arises from a lack of proton data and a poor understanding of nuclear corrections necessary to interrupt nuclear targets (even deuterium). The absolute *proton-proton* Drell-Yan data from this experiment will be free from these uncertainties. In the intermediate- x ($0.1 < x < 0.45$) deuterium absolute cross section data will be provide a direct

¹The subscript p is used to denote the proton's parton distributions (as opposed to n for the neutron). From here on, unless otherwise needed for clarity, $\bar{d}(x)$ and $\bar{u}(x)$ will refer to the distributions in the proton and the subscript p will be omitted.

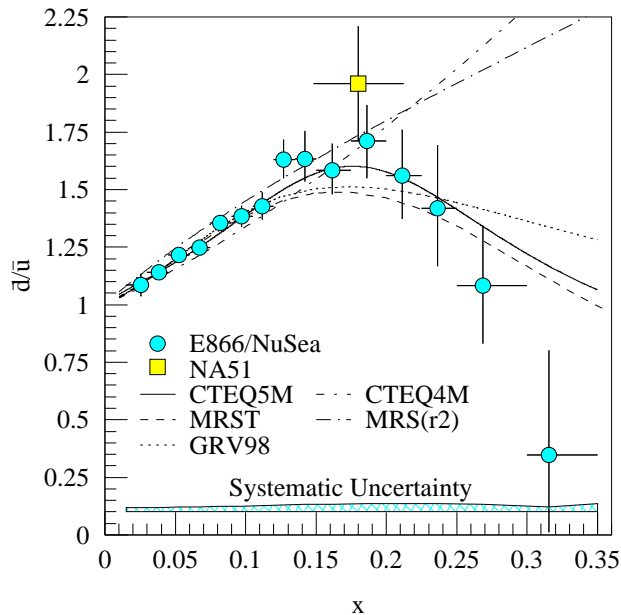


Figure 1: FNAL E866 results [11] for the x -dependence of the ratio $\bar{d}(x)/\bar{u}(x)$ of the proton at a mass scale of 7.35 GeV. The square point is the NA51 result ($Q = 5.2$ GeV) [8]. Also shown are parameterizations of this ratio from CTEQ4M [1] and MRS(r2) [4] prior to the FNAL E866 results and parameterizations from CTEQ5M [2], MRST [5] and GRV98 [6] which have included the E866 data in the fitting procedure.

measurement of $\bar{d}(x) + \bar{u}(x)$, a quantitatively which was previously only measured through neutrino DIS on heavy nuclei.

Additionally, proton-induced Drell-Yan cross sections on nuclear targets will be measured. The present knowledge of the flavor dependence of the nuclear parton distributions limits the understanding of the nuclear dependences that have been observed. Many models of nuclear binding expect an increase in the antiquark distributions in a nucleus (e.g. [12]). This increase has not, as yet, been observed. With the greater reach at higher x , E906 will be able to significantly constraint these models. Measurements of the absolute Drell-Yan cross sections on nuclei will be able to provide a direct comparison between the neutrino and the Drell-Yan deuterium data and determine how nuclear effects might influence the interpretation of neutrino determination of $\bar{d}(x) + \bar{u}(x)$.

The data from nuclear targets will also be used to determine the energy loss of a quark traveling through a cold nucleus. The initial state beam quark will interact strongly and loose energy as it penetrates the nucleus before annihilating. The energy loss results in an apparent shift in the observed parton momentum fraction, x of the interacting quark. By comparing measurements on differently sized nuclei, the energy loss can be determined. Previous Drell-Yan experiments have placed limits on the energy loss [13], but with the higher statistics and increased sensitivity from the lower beam energy, this experiment will be able to quantitatively distinguish between competing models. The entire physics program of the experiment is presented in section 2.

The E906 experiment has already been approved by the Fermilab PAC for the next fixed target run (along with the CKM experiment [14]). The design of the E906 experimental apparatus relies heavily on our previous experience in Fermilab E605, E772, E789 and E866/NuSea. Much of the detector hardware already exists and was used in these previous experiments or in Fermilab E871.

Because of the lower energy, however, it will be necessary to fabricate coils for a new magnet. Details of the detector are given in section 3 and additional cost and scheduling information are in section 4.

2 Discussion of Physics

To lowest order the Drell-Yan process, virtual photon production in hadron-hadron collisions, depends on the product of quark and antiquark distributions in the beam and target:

$$\frac{d^2\sigma}{dx_1 dx_2} = \frac{4\pi\alpha^2}{9sx_1x_2} \sum_i e_i^2 \left[q_{1i}(x_1, Q^2)\bar{q}_{2i}(x_2, Q^2) + \bar{q}_{1i}(x_1, Q^2)q_{2i}(x_2, Q^2) \right]. \quad (1)$$

where q_{1i} (q_{2i}) are the beam (target)² quark distributions and the sum is over all quark flavors (u, d, s, c, b, t). The fraction of the longitudinal momentum of the beam (target) carried by the participating quarks are $x_{1(2)}$. The squared total energy of the beam-target system is $s = 2m_2E_1 + m_1^2 + m_2^2$ where E_1 the energy of the beam hadron and m_1 (m_2) the rest masses of the beam (target) hadron. In the case of nuclear targets, it is assumed that the reaction takes place on a component nucleon, $m_2 = M_n$, where M_n is the nucleon mass, and the momentum fraction, x_2 refers to the fractional momentum of the parton relative to the interacting nucleon.

The sensitivity of the Drell-Yan process to the antiquark distributions of the target and beam is clear from examining equation 1. At large values of x , the parton distributions are dominated by the valence distributions and at small x by the sea distributions. Thus, in the limit of large x_1 and small x_2 , the cross section is dominated by the first term—the annihilation of *beam quarks* with *target antiquarks*, providing direct sensitivity to the antiquark sea of the target nuclei.

E906 will extend the measurements made by E866 to relatively large x_2 where the antiquark distributions are small. For this, beams from the 120 GeV/c Fermilab Main Injector have two primary advantages compared with previous 800 GeV/c measurements:

- For fixed x_1 and x_2 the cross section is proportional to $1/E_b$, where E_b is the incident beam energy, as shown in equation 1. A 120 GeV/c Main Injector experiment will have a factor of nearly 7 times larger cross sections compared with previous experiments which used an 800 GeV/c extracted Tevatron beam.
- Practical limitations in the acceptable luminosity for these experiments are radiation protection limits and the single muon rates in the detectors. To the extent that the radiation dose scales as beam power, one can take approximately 7 times the luminosity for the same beam power at 120 GeV/c relative to 800 GeV/c. In E866 at 800 GeV/c, J/ψ events from the beam dump were a significant contribution to the muon singles rates. At 120 GeV/c the total J/ψ production cross sections fall by an order of magnitude when compared with 800 GeV/c.

The combination of these effects is expected to allow a factor of nearly 50 improvement in the number of recorded events at high x_2 when compared with previous Drell-Yan experiments.

The kinematics of the virtual photon in the Drell-Yan process—longitudinal center of mass momentum p_{\parallel}^{γ} , transverse momentum p_T^{γ} and mass M_{γ} —are determined by measuring its the two-muon decay. These quantities determine the momentum fractions of the two interacting quarks:

$$x_F = \frac{p_{\parallel}^{\gamma}}{p_{\parallel}^{\gamma, \max}} \approx x_1 - x_2 \quad (2)$$

²The subscripts 1 and 2 will be used throughout this proposal to denote the beam and target, respectively.

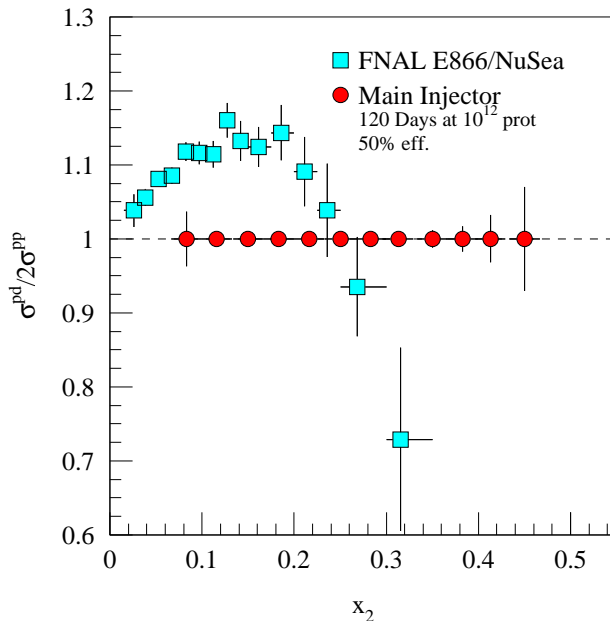


Figure 2: FNAL E866 results[9, 11] for the ratio of $\sigma^{pd}/2\sigma^{pp}$. The statistical uncertainties expected for the measurement proposed here are shown as the error bars on the solid circles (which are arbitrarily plotted at 1.0). The systematic errors are estimated to be less than 1%.

$$x_1 x_2 s \approx M_\gamma^2 \quad (3)$$

where $p_{\parallel}^{\gamma, \max}$ is the maximum kinematic value p_{\parallel}^{γ} can have.

The expected statistical precision with which the ratio $\sigma^{pd}/2\sigma^{pp}$ will be measured in this experiment is shown in Fig. 2 along with the E866 measurements. It is apparent that a high luminosity Main Injector experiment can extend the x range of our knowledge of $\bar{d}(x)/\bar{u}(x)$ up to $x \approx 0.45$.

As can be seen by comparing the $\bar{d}(x)/\bar{u}(x)$ curves shown in Fig. 1, the inclusion of the E866 data completely changed the parameterization of the antiquark sea for $x > 0.20$. In determining the anti-quark content of the proton sea, the parton distribution fits have simply parameterized the E866 data with a convenient algebraic form. While the chosen form reproduces the Drell-Yan data well, the statistical uncertainty on the data still allows for up to a 50% variation at $x = 0.3$ compared with only a few percent uncertainty up to $x = 0.4$ which would be achieved by the present proposal, as shown in figure 2.

2.1 Parton Distributions: $\bar{d}(x)/\bar{u}(x)$ of the Proton

The ratio of $\bar{d}(x)/\bar{u}(x)$ in the proton may be determined by measuring the ratio of proton induced Drell-Yan on deuterium to that on hydrogen. Both Fermilab E866 and CERN NA51 used this method to determine $\bar{d}(x)/\bar{u}(x)$. To extract this from the measured ratio, nuclear effects in deuterium were ignored—its cross section was treated as the sum of the free proton and free neutron cross sections and charge symmetry was then used to equate \bar{d}_p to \bar{u}_n and \bar{u}_p to \bar{d}_n . Ignoring the strange and heavier quark contribution and taking the limit that $x_1 \gg x_2$ (*i.e.* the beam antiquark-target quark contribution is small) the ratio of Drell-Yan cross sections can be written

as:

$$\frac{\sigma^{pd}}{2\sigma^{pp}} \Big|_{x_1 \gg x_2} \approx \frac{1}{2} \left[\frac{1 + \frac{d(x_1)}{4u(x_1)}}{1 + \frac{d(x_1)}{4u(x_1)} \frac{\bar{d}(x_2)}{\bar{u}(x_2)}} \right] \left[1 + \frac{\bar{d}(x_2)}{\bar{u}(x_2)} \right]. \quad (4)$$

Observing that $d(x) \ll 4u(x)$, this expression simplifies even further to

$$\frac{\sigma^{pd}}{2\sigma^{pp}} \Big|_{x_1 \gg x_2} \approx \frac{1}{2} \left[1 + \frac{\bar{d}(x_2)}{\bar{u}(x_2)} \right]. \quad (5)$$

This expression illustrates the sensitivity of the experimental ratio to $\bar{d}(x)/\bar{u}(x)$, the actual extraction of $\bar{d}(x)/\bar{u}(x)$ will be performed using equation 1 and verified with full next-to-leading order (NLO) cross section calculations, as was done in E866.

2.1.1 Origins of the Nucleon Sea

While providing direct input to the parton distribution fits, the ultimate impact of this experiment will be to provide a better understanding on the physical mechanism which generates the sea of the proton. The $\bar{d}(x) - \bar{u}(x)$ difference, shown in Fig. 3, is a pure flavor non-singlet quantity: its integral is Q^2 independent [15] and its Q^2 evolution at leading order does not depend on the gluon distribution of the proton. Early expectations were that Pauli blocking due to the extra valence u quark in the proton would lead to a suppression of $g \rightarrow u\bar{u}$ which would contribute significantly to differences in the light sea [16]. These expectations were not, however, borne out by calculations [17, 18] (though this point is still debated in the literature [19]). In perturbative QCD, differences between the $\bar{d}(x)$ and $\bar{u}(x)$ distributions arise only at second order and are calculated to be very small [17]. The large differences seen in Figs. 1, 2 and 3 must be non-perturbative in nature and are likely explained in terms of collective degrees of freedom of QCD at low energy.

There are three significant non-perturbative approaches that can accommodate large differences in $\bar{d}(x) - \bar{u}(x)$: (1) hadronic models of the meson cloud of the nucleon, (2) chiral quark models which couple mesons directly to constituent quarks and (3) instanton models. Figure 3 illustrates calculations for representative examples of each of these models. An intriguing feature is that in each of these models the flavor and spin distributions of the proton are intimately linked. As these non-perturbative models are considered, it is important to remember that they must be combined with perturbative sources to generate the entire quark sea of the proton.

The pion cloud model has a tantalizing simplicity and does explain basic features of the data. A proton wave function containing sizable virtual $|n\pi^+\rangle$ Fock states will have an excess of \bar{d} -quarks from the valence quarks in the π^+ . The difficulty in this approach is finding justification to truncate the hadronic expansion [23]. Most calculations include contributions for $|N\pi\rangle$ and $|\Delta\pi\rangle$ states (*e.g.* Ref. [24]). The pion-nucleon and pion-delta coupling constants ($g_{\pi NN}$ and $g_{\pi N\Delta}$) are well known, so the primary difference among calculations is the treatment of the πNN and $\pi N\Delta$ vertex factors. Using “not unreasonable” vertex functions (dipole vertex functions with cut offs, Λ , of $\Lambda_{\pi NN} = 1.0$ GeV and $\Lambda_{\pi N\Delta} = 0.8$ GeV) reasonable agreement with the data [10] is found as show in the solid curve of Fig. 3. The resulting probabilities for the $|N\pi\rangle$ and $|\Delta\pi\rangle$ admixture lead to a prediction for the difference in total spin carried by the u quarks (Δu) and the d quarks (Δd), $\Delta u - \Delta d = G_A$ of approximately 1.5 [10], providing part of the reduction from the quark model value of 5/3.

Chiral field theories suggest that the relevant degrees of freedom are constituent quarks, gluons and Goldstone bosons. Processes such as $u \rightarrow d\pi^+$ and $d \rightarrow u\pi^-$ generate a flavor asymmetry in the sea simply because there are more up than down quarks in the proton. Two predictions of

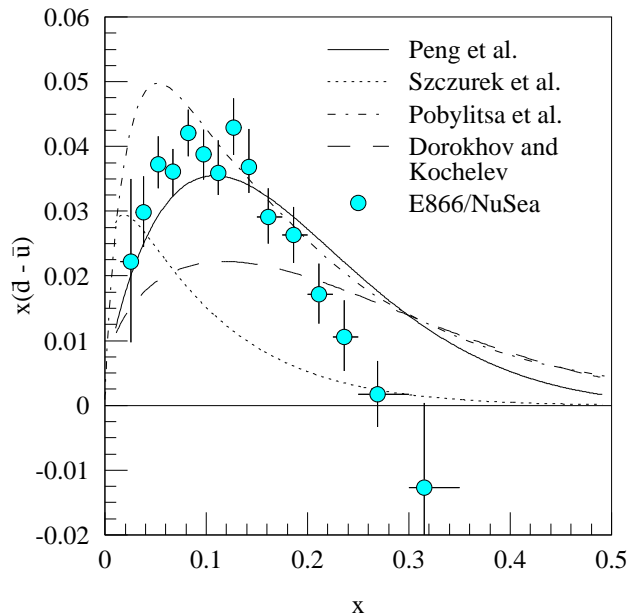


Figure 3: FNAL E866 results [9, 10, 11] for $x [\bar{d}(x) - \bar{u}(x)]$ at a mass scale of 7.35 GeV. The curves represent four model calculations of $x [\bar{d}(x) - \bar{u}(x)]$. The solid curve is a meson-cloud model calculation including nucleons, deltas and pions [10]. The dotted and dot-dashed curves are a chiral quark models [20, 21] and the long-dashed curve is an instanton inspired parameterization [22].

$\bar{d}(x) - \bar{u}(x)$ from chiral models are shown in Fig. 3 at the dotted and dot-dashed curves. Clearly the model of Szczurek *et al.* [20] is too soft. The chiral quark-soliton model of Pobylitsa *et al.* [21] better reproduces the measured $x [\bar{d}(x) - \bar{u}(x)]$ distribution for $x > 0.08$, but overestimates the asymmetry at small x .

Instanton effective Lagrangians imply coupling at the tree level between instantons and the valence quarks which leads to a $\bar{d}(x) - \bar{u}(x)$ difference. This raises the intriguing possibility that Drell-Yan measurements could provide experimental information on these theoretically very useful but seemingly experimentally inaccessible constructs. Within the framework of the t'Hooft SU(2) effective Lagrangian [25] (which is of the form $\bar{u}_R u_L \bar{d}_R d_L + \bar{u}_L u_R \bar{d}_L d_R$ where the subscripts R and L label the quark helicity) the u quarks generate a $\bar{d}d$ sea and the helicity of the valence quarks is screened [22]. (A flavor SU(3) Lagrangian would also generate $s\bar{s}$ pairs.) Dorokhov and Kochelev fit the NMC measurement of the $\bar{d}(x) - \bar{u}(x)$ integral to a form parameterized to have the expected asymptotes which is shown as the long-dashed curve on Fig. 3. The $\bar{d}(x) - \bar{u}(x)$ difference observed by E866 does not show the transverse momentum (p_T) dependence expected in Ref. [22], however. One set of predictions is the relations between the instanton contributions (subscript I in Eq. 6) of the spin and flavor matrix elements, for example:

$$\bar{d}_I(x) - \bar{u}_I(x) = \frac{3}{5} [\Delta u_I(x) - \Delta d_I(x)] \quad (6)$$

It is interesting to note that while this approach gives a reduction in the total spin carried by the quarks in the nucleon, it implies an increase in $\Delta u_I(x) - \Delta d_I(x)$ while in the other models an increase in the flavor asymmetry causes a decrease in $\Delta u(x) - \Delta d(x)$.

As mentioned earlier, none of these models consistently incorporate the flavor symmetric sea and consequently all substantially over predict the ratio of $\bar{d}(x)/\bar{u}(x)$ for $x > 0.23$. Unfortunately

the statistical uncertainty on the E866 data becomes large in this region. The pion models tend to level off at a predicted $\bar{d}(x)/\bar{u}(x)$ between 1.5 and 5 (depending on the baryons and mesons included in the calculations) until $x > 0.5$ where the ratio begins to decrease slowly to unity. The instanton model predicts a ratio of $\bar{d}(x)/\bar{u}(x) \approx 4$ at high x . One possible interpretation of the E886 results is that the perturbative gluon mechanism begins to re-establish its dominance over the non-perturbative mechanisms at a lower value of x than previously expected, indicating a larger gluon component in the proton. The gluon distribution at high x is, at present, poorly constrained and changed considerably from MRS(r2) [4] to MRST [5] with a change in the treatment of the fixed target prompt photon data. In addition, recent collider inclusive jet cross sections suggest a stronger gluon content to the proton than is present in the parameterizations [26].

2.1.2 Interpretability of the Results: QCD factorization

The interpretability of Drell-Yan results as direct measures of the parton distributions is based on the QCD factorization theorems [27, 28]. Bodwin, Brodsky and Lepage [28] give the condition for the minimum beam momentum P_{\min} below which initial state QCD interactions become important as:

$$P_{\min} \approx \frac{p_T A^{2/3}}{x_1} \quad (7)$$

A conservative estimate of $\langle p_T^2 \rangle \approx 0.4 \text{ GeV}^2$ (Ref. [28] uses 0.25 GeV^2) yields a typical transverse hadronic scale p_T on the order of 0.6 GeV and a minimum beam momentum of 23 GeV for $x_1 > 0.3$ and a calcium target, comfortably below the $120 \text{ GeV}/c$ considered here.

2.1.3 Competing Measurements of \bar{d}/\bar{u}

We see no significant competition for measurements of the flavor dependence of antiquark distributions in this x range. The classes of experiments with potential sensitivity are neutrino deep inelastic scattering (ν DIS), semi-inclusive deep inelastic scattering (SIDIS), electroweak boson production at pp colliders and other Drell-Yan measurements. Each will be considered briefly in turn.

CCFR and NuTeV [29, 30] have accumulated significantly more statistics in ν - and $\bar{\nu}$ DIS which will allow a more precise determination of $(\bar{d} + \bar{u})$ but the uncertainties of using a heavy target will remain. On an almost isoscalar target, there is little sensitivity to $(\bar{d} - \bar{u})$.

The flavor dependence of the parton fragmentation functions is used in SIDIS to disentangle the contributions of the different parton distributions. The HERMES collaboration at DESY has used SIDIS to study the flavor dependence of the sea [31]. The HERMES results agree well with the E866 results but have factors of 5 larger error bars, as shown in Fig. 4. SIDIS most directly measures

$$\frac{\bar{d}(x) - \bar{u}(x)}{u(x) - d(x)} = \frac{J(z) [1 - r(x, z)] - [1 + r(x, z)]}{J(z) [1 - r(x, z)] + [1 + r(x, z)]}, \quad (8)$$

with

$$r(x, z) = \frac{N_p^{\pi^-} - N_n^{\pi^-}}{N_p^{\pi^+} - N_n^{\pi^+}}. \quad (9)$$

Here, $J(z)$ depends on the fragmentation functions and z is the fraction of the energy of the virtual photon carried by the hadron. At high x where the difference of antiquark distributions is much smaller than the difference of quark distributions, one must measure differences of several comparable size numbers. Additionally, the systematic uncertainty due to the fragmentation physics is also an issue. The experiments which can improve these measurements are HERMES and COMPASS, both of which concentrate on polarized structure function measurements. While HERMES will

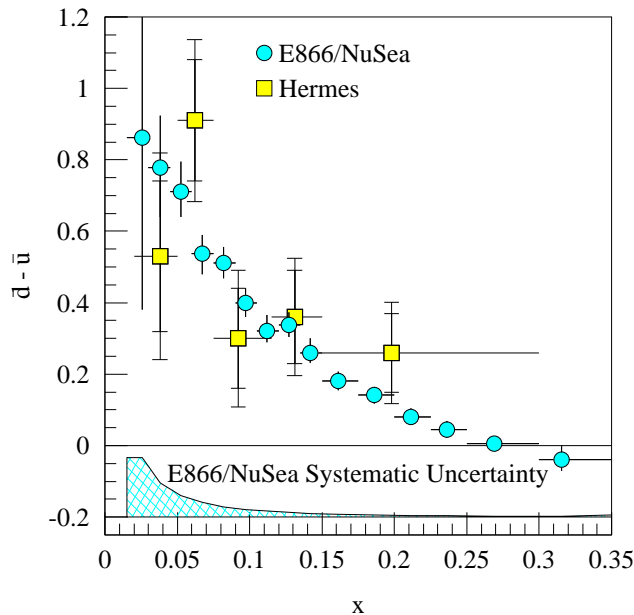


Figure 4: Measurement of $\bar{d}(x) - \bar{u}(x)$ from HERMES [31] compared with the measurements of FNAL E866/NuSea. The inner error bars on the HERMES data points represent the statistical uncertainty while the outer error bars represent the statistical and systematic uncertainty added in quadrature. The uncertainty shown on the E866/NuSea data is statistical, with the common systematic uncertainty shown by the band at the bottom.

likely increase their data set by another factor of five in dedicated unpolarized running, they will not be able to extend their x range significantly to higher x . The COMPASS experiment at CERN could do similar semi-inclusive SIDIS measurements. To date they have not proposed dedicated unpolarized running with rapid interchange of pure hydrogen and deuterium targets. There have been proposals for similar measurements at Jefferson Laboratory for with both the current facility [32] (deferred) and the upgraded 12 GeV facility [33]. While these proposals have a significant reach in x , the theoretical interpretation of the data in terms of $\bar{d}(x) - \bar{u}(x)$ is not as clean as for Drell-Yan, and their agreement with Drell-Yan data may be viewed as a test of factorization at these energies.

The production of W bosons in p-p collisions does offer sensitivity to the antiquark distributions. At the LHC one only has sensitivity for the x range considered here at the highest rapidities ($y > 4$). However at RHIC higher x values are quite relevant and plans are underway to use the W decay asymmetry in single spin asymmetries to study the antiquark polarization. Since the RHIC detectors have limited kinematic coverage and these events have missing transverse energy, the parton level kinematics of each event are not well determined and one averages over a significant x region. With the antiquark distributions falling rapidly, the lepton asymmetry yields are dominated by lower x values. We have discussed the plans with members of the STAR and PHENIX collaborations at RHIC. They concluded that they will not be sensitive to the antiquark distributions at $x > 0.2$.

In contrast to processes like SIDIS, the Drell-Yan measurement of \bar{d}/\bar{u} has much smaller systematic errors and acceptance corrections. We know of no other planned fixed target Drell-Yan measurements in the near future. In the long term, lower energy, high intensity machines such as

the Japanese hadron facility could address this physics. We consider the energy of the main injector to be the optimum combination of reliable interpretation and attainable precision.

Experts like James Sterling [34] have given their strongest support to our proposal as the best way to measure the flavor dependence of the antiquark distributions at high x . Again we see no serious competition for this experiment in the near future.

2.2 Measurements of Other Parton Distributions

In addition to the Drell-Yan ratio measurement, the absolute Drell-Yan proton-hydrogen and proton-deuterium cross sections will be determined. These measurements will be sensitive to the properties of the beam proton over the range $0.3 < x_1 \leq 0.9$ and of the target over the range $0.1 < x_2 < 0.45$. The deuterium absolute cross section can be used to determine the magnitude of the anti-quark sea, $\bar{d}(x) + \bar{u}(x)$. Until now, the parton distribution fits obtained sensitivity to the magnitude of the sea distribution at high x from the CCFR neutrino measurements on iron [29], the E605 Drell-Yan measurements on Cu [35] and the E772 Drell-Yan measurements on deuterium [36]. The E605 and E772 measurements will soon be superseded by E866 absolute Drell-Yan cross section results [37]. The extracted magnitude of $(\bar{d} + \bar{u})$ depends on differences between neutrino, anti-neutrino and electron/muon deep inelastic scattering results. The nuclear corrections, which can be different for valence and sea quarks, are a significant uncertainty in these comparisons. One of the primary advances of E906 will be absolute p - p , p - d and p - A Drell-Yan cross sections at high x and a precise measurement of the nuclear dependence of the \bar{u} distribution at these x regions.

When viewed in as a function of the beam momentum fraction x_1 , the absolute cross section data provide information about the partonic structure of the beam proton. As $x \rightarrow 1$, the parton distributions are poorly determined. This is due to a lack of proton data and due to significant theoretical uncertainties in the interpretation of nuclear data—even in deuterium [38, 39]. Drell-Yan proton-proton data will be completely free from these uncertainties, and Drell-Yan proton-deuterium data will probe high- x of the beam proton and intermediate- x of the target deuterium, where these nuclear effects are understood. An examination of Fermilab E866/NuSea data [37] indicate that the CTEQ6 [3] parameterizations produce a much larger NLO cross section than is actually seen at high- x as shown in Fig. 5. This is most likely due to one of two effects. CTEQ6 assumes that $d/u|_{x \rightarrow 1} \rightarrow 0$. This is based on the belief $S = 0$ diquarks (where S represents the total spin of the diquark) dominate the proton wave function as $x \rightarrow 1$. Other models, however produce $d/u|_{x \rightarrow 1}$ that range from 1/5 to 1/2 [38]. In this high- x region, Drell-Yan essentially measures $4u(x) + d(x)$. An increase in d/u at high- x could bring the NLO cross section calculation into agreement with the data. Alternatively, an overall decrease in the strength of the valence distribution as $x \rightarrow 1$ would also bring the calculation into agreement with the measured cross section. The E906 experiment will significantly increase the amount of data available at high- x . Fig. 5 shows the expected statistical uncertainty which will be achieved by E906.

2.3 Antiquark Distributions of Nuclei

The distributions of partons within a free nuclei differ from those of a nuclei bound within a heavy nucleus, an effect first discovered by the EMC collaboration in 1983 [40]. Much of the data on nuclear dependencies comes from charged lepton deep inelastic scattering (DIS) experiments, which are sensitive only to the charge-weighted sum of all quark distribution. The antiquark distributions at large x are determined primarily from ν DIS on heavy targets, but there is no similar high statistics ν DIS data on light (hydrogen or deuterium) targets. Nuclear effects in the sea quark distributions may be entirely different than those in the valence sector, and indeed, Drell-Yan data

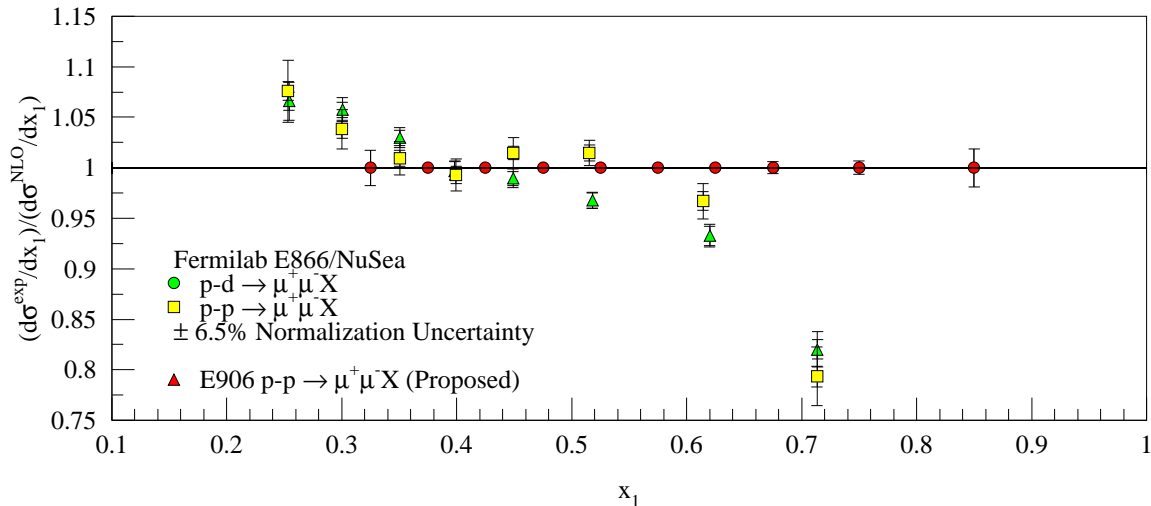


Figure 5: The ratio of Drell-Yan cross section measured by Fermilab E866/NuSea [37] for proton-deuterium (squares) and proton-proton (triangles) to calculated NLO cross section based on the CTEQ6 [3] parton distributions. The inner error bars are statistical only. The outer error bars are a *linear* sum of statistical and point-to-point systematic uncertainties. The deficit at high- x may indicate that $d/u|_{x \rightarrow 1} > 0$ contrary to the assumptions on which CTEQ6 was based. The circles show the statistical uncertainties which will be obtained with E906, arbitrarily plotting the ratio at 1.

from E772 show no antishadowing, although, with limited statistics [41]. High precision Drell-Yan measurements at x larger than E772 could access would provide extremely valuable new information on the nuclear dependence of parton distributions. In addition, the absolute deuterium and nucleus cross section measurements will give a direct measurement of the strength of the sea ($\bar{d} + \bar{u}$) and its nuclear dependence, providing direct comparisons to neutrino-nucleus data which was previously used to determine this quantity. The expected statistical precision of the proposed measurement is shown in Fig. 6, compared with the existing Drell-Yan and DIS results on the ratios of calcium to deuterium. E906 will be able to precisely measure nuclear effects through out the antishadowing and into the “EMC effect” region.

In the context of nuclear convolution models, virtual pion contributions to nuclear structure functions were expected to lead to sizable increases in sea distributions of the nuclei compared with deuterium. This expectation was convincingly shattered by the E772 Drell-Yan measurements [41], as shown in Fig. 7, which found little nuclear dependence except in the shadowing region. The non-observation of evidence for nuclear pions or a pion excess calls into question the most widely believed traditional meson-exchange model [42] of the nucleus. The absence of the anti-quark excess associated with pion exchange is a fundamental problem for nuclear physics. The expected enhancement to the sea is illustrated in Fig. 8, which shows the expected ratio of \bar{u} in iron to \bar{u} in deuterium which is based on the nuclear convolution model calculations by Coester [43]. This should be directly comparable to the iron to deuterium ratio measured by E772. More recent calculations, made in light of the E772 data, predict a smaller nuclear dependence, consistent with the statistical uncertainties of E772 [44, 45, 46]. Unfortunately, for $x > 0.2$, the E772 statistical uncertainties allow some freedom for these models. At $x \approx 0.3$ these newer models have nuclear effects of the order 5 to 15% in the Drell-Yan ratio. E906 will provide the sensitivity needed to

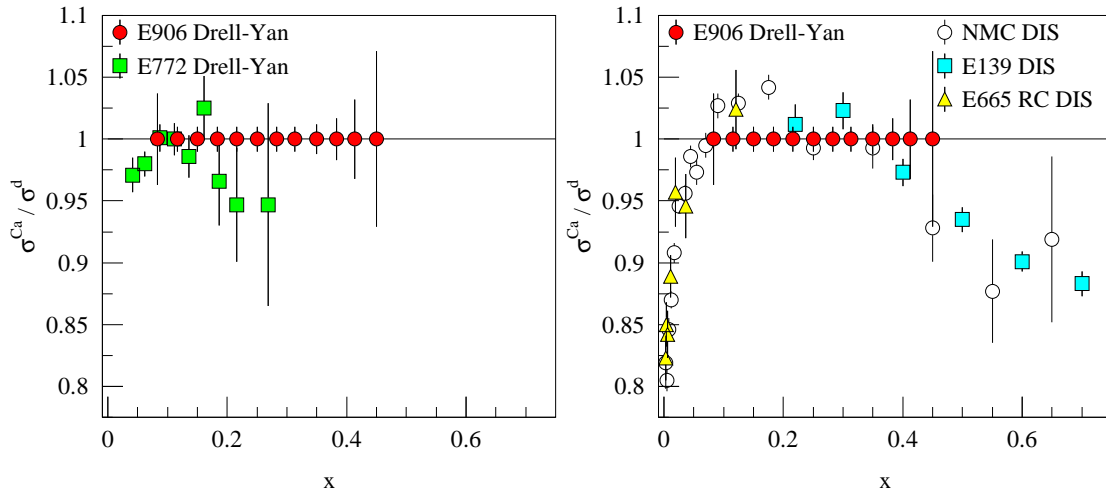


Figure 6: FNAL E772 Drell-Yan results (left) and a compilation of deep inelastic scattering (right) results on the ratio of cross sections of calcium to deuterium, compared with the statistical uncertainties of the proposed measurement (which are arbitrarily plotted at 1.0). The systematic error is expected to be less than 1%.

see the reduction in the nuclear sea distributions predicted in the Q^2 rescaling models [44] and differentiate this from other models which predict an enhancement in the Drell-Yan ratio.

Finally, the nuclear target data will constrain possible nuclear effects in the \bar{d}_p/\bar{u}_p measurement. A large rise in the nuclear ratio would provide an important alert that nuclear effects may be important in the deuterium to hydrogen ratio.

2.4 Partonic Energy Loss

Parton energy loss is a fundamental process within QCD that has significant impact on the physics of relativistic heavy-ion collisions. The magnitude of the initial energy loss in the heavy-ion collision determines the ultimate density that is achieved. Furthermore, anomalous energy loss of fast partons (“jet quenching”) has been identified as a tool to measure the gluon density of the high temperature medium which is created at RHIC and a possible signature for the creation of a quark-gluon plasma.

The PHENIX collaboration [47] has reported evidence for the suppression of high- p_T π^0 s and both the STAR [48] and PHENIX [49] collaborations have reported evidence for the suppression of high- p_T charged hadrons in $Au-Au$ collisions at $\sqrt{s_{NN}} = 130$ GeV. The STAR collaboration [50] has also identified large azimuthal anisotropies in the production of high- p_T charged hadrons in $Au-Au$ collisions at $\sqrt{s_{NN}} = 130$ GeV. At the recent Quark Matter 2002 conference [51], both collaborations presented first results of similar studies for $Au-Au$ collisions at $\sqrt{s_{NN}} = 200$ GeV. The PHENIX data now reach to $p_T \approx 10$ GeV/c and include a π^0 reference spectrum taken with the same detector. The STAR data now reach to $p_T \approx 12$ GeV/c and include evidence for the suppression of back-to-back jets in central $Au-Au$ collisions. These results, taken together, provide clear evidence for energy loss of high- p_T partons or their hadronic fragments in the high-density medium produced in $Au-Au$ collisions at RHIC. However, detailed interpretation will require understanding several additional competing effects—including initial- and final-state multiple scattering, gluon shadowing, radial and elliptical flow—as well as the energy loss of fast partons in normal nuclear matter.

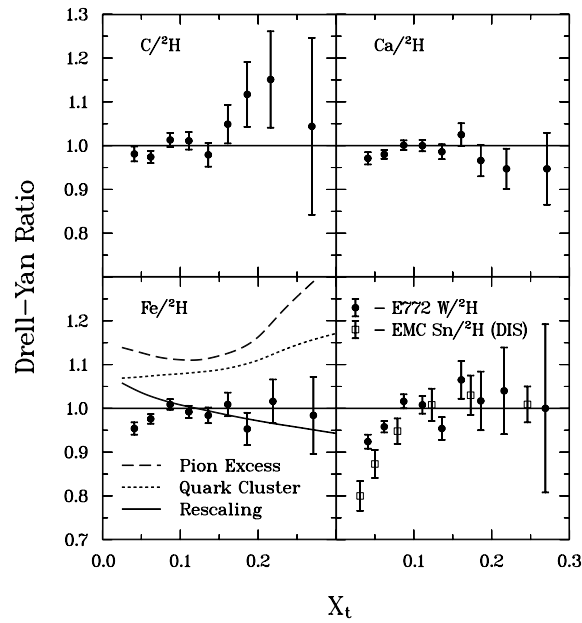


Figure 7: E772 measurements of the ratio of Drell-Yan cross sections on nuclear targets to deuterium [41].

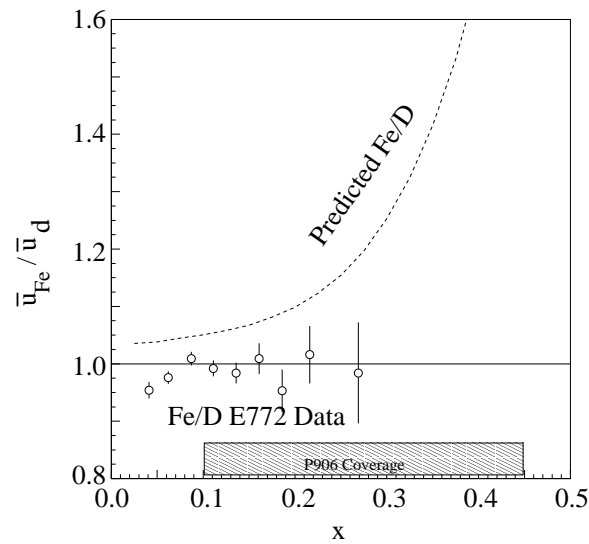


Figure 8: Ratio of \bar{u} iron to \bar{u} in deuterium as calculated by Coester [43] including both nuclear motion and pion contributions, which should be directly comparable to the E772 data [41]. The shaded box shows the x coverage of this proposal.

The Drell-Yan process provides an excellent means to study the interactions of fast partons traversing cold nuclei since the dimuon in the final state does not interact strongly with the partons in the medium. Thus, it can be used to estimate the energy loss of fast quarks in cold nuclear matter, thereby establishing a baseline for the energy loss that would be expected during a heavy-ion collision even without formation of a quark-gluon plasma. Both E772 [41] and E866 [13] measured the nuclear dependence of Drell-Yan dimuon production in 800 GeV/c p - A collisions, and the E866 results have been analyzed to search for evidence of energy loss of the incident quark as it traversed the nucleus prior to the hard scattering [13].

Three different forms for this energy loss have been proposed, each of which can be expressed in terms of the average change in the incident-parton momentum fraction prior to the collision, Δx_1 , as a function of target atomic mass (A). Gavin and Milana [52] adopted a form

$$\Delta x_1 = -\kappa_1 x_1 A^{1/3}, \quad (10)$$

based on an analogy to the transverse spin asymmetry in direct photon production. Brodsky and Hoyer [53] used an analogy to the photon bremsstrahlung process to obtain a form for gluon radiation, leading to an initial-parton energy loss

$$\Delta x_1 \approx -\frac{\kappa_2}{s} A^{1/3}. \quad (11)$$

They also noted that elastic scattering should make a similar contribution to the energy loss. The formulation developed by Brodsky and Hoyer was extended by Baier *et al.* [54]. They found that the energy loss of sufficiently energetic partons depends on a characteristic length and the broadening of the squared transverse momentum of the parton. For finite nuclei, both factors vary as $A^{1/3}$, so Baier *et al.* predict

$$\Delta x_1 \approx -\frac{\kappa_3}{s} A^{2/3}. \quad (12)$$

In each of these three equations, κ is a constant that sets the overall scale of the energy loss.

In all three cases, the signature for incident-parton energy loss is a modification of the Drell-Yan cross section per nucleon on a heavy nucleus as a function of x_1 . However, the E866 nuclear dependence data were taken at relatively small x_2 ($\langle x_2 \rangle = 0.038$), where DIS experiments show clear evidence for nuclear shadowing. In addition, the Drell-Yan acceptance in E866 introduced a strong anti-correlation between x_1 and x_2 . Thus, it was essential to correct the data for the effects of nuclear shadowing. The EKS98 shadowing parameterization [55] was designed to fit the observed nuclear dependence of deep-inelastic scattering over a broad range of x and the nuclear dependence of Drell-Yan scattering observed by E772 at $x_2 > 0.08$, while simultaneously conserving baryon number and momentum. It gives a very good description of the nuclear dependence of the Drell-Yan cross section per nucleon at small x_2 observed in E866. Thus, EKS98 was used to correct the E866 data for nuclear shadowing.

The small residual nuclear dependence observed in E866 as a function of x_1 was then used to set upper limits on the incident-parton energy loss in each of the three models above. The fits are shown in Fig. 9. E866 found that the fractional energy loss of the incident quarks is less than 0.14%/fm (1σ), when using the model of Gavin and Milana. The incident quarks lose energy at a constant rate of less than 0.44 GeV/fm, when using the model of Brodsky and Hoyer, and the observed energy loss of the incident quarks within the model of Baier *et al.* is $\Delta E < 0.046 \text{ GeV/fm}^2 \times L^2$, where L is the quark propagation length through the nucleus. These upper limits on the energy loss are tighter than previous direct constraints.

An alternative approach has been adopted to determine incident-parton energy loss in a recent reanalysis [56] of the E772 and E866 Drell-Yan nuclear dependence studies. This work fits

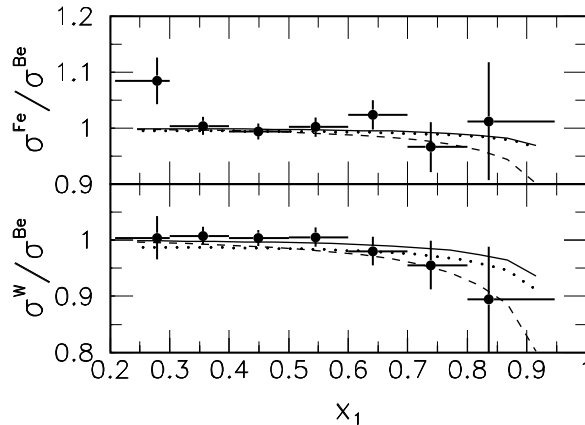


Figure 9: E866 ratios of the Drell-Yan cross section per nucleon versus x_1 for Fe/Be (upper panel) and W/Be (lower panel), corrected for shadowing [13]. The solid curves are the best fit using the energy loss form in Eq. 10, and the dashed curves show the one standard deviation upper limits. The dotted curves show the one standard deviation upper limits using the energy loss form in Eq. 12. The upper limit curves using the energy loss form in Eq. 11 are essentially identical to those using the form in Eq. 12.

the Drell-Yan nuclear dependence with the combination of a “first-principles” calculation of the nuclear shadowing in Drell-Yan scattering, based on the coherence length of $q \leftrightarrow q\gamma^*$ fluctuations as observed in the target nucleus rest frame, and a colored-string model for parton energy loss. It concludes that the average incident-parton energy loss is $2.73 \pm 0.37 \pm 0.5$ GeV/fm, in clear contradiction to the less than 0.44 GeV/fm result from the most similar E866 analysis. Approximately half of this difference originates from different treatments of the path length through the nuclear matter. The E866 analysis took the path length to be the average propagation distance within the nucleus prior to the hard scatter that produces the Drell-Yan pair, whereas the recent E772 and E866 data reanalysis takes the path length to be the average propagation distance from the first inelastic scattering, when the colored string is formed, until the hard scatter occurs. The rest of the difference can be traced ultimately to the two different treatments of nuclear shadowing. In particular, the “first-principles” calculation predicts much less shadowing than the EKS98 parametrization and, thus, requires considerably more energy loss to fit the experimental data.

At present, it is unclear which approach to evaluate the shadowing is more appropriate for the existing experiments. The coherence-length approach is based on well-defined QCD principles and is particularly attractive at very small x_2 . Similar calculations of shadowing in deep-inelastic scattering do a very good job of describing the data at small x . However, for $x > 0.04$, the coherence-length calculations fail to reproduce the nuclear dependence observed in deep-inelastic scattering. This is notable because most of the E772 Drell-Yan events and nearly half of the E866 Drell-Yan events have $x_2 > 0.04$. Furthermore, the large apparent energy loss found using the coherence-length approach appears to be inconsistent with the initial results from RHIC. It is also inconsistent with two other recent determinations of the energy loss of fast quarks in cold nuclear matter: 0.20 ± 0.15 GeV/fm from a combined fit to the E866 (p -A) and NA3 (π^- -A) Drell-Yan data [57] and 0.5 GeV/fm from a study of semi-inclusive DIS data from HERMES [58].

In contrast to the “first-principles” shadowing calculations, EKS98 is based primarily on *ad hoc* parameterizations of the nuclear dependence seen in deep-inelastic scattering that have only limited

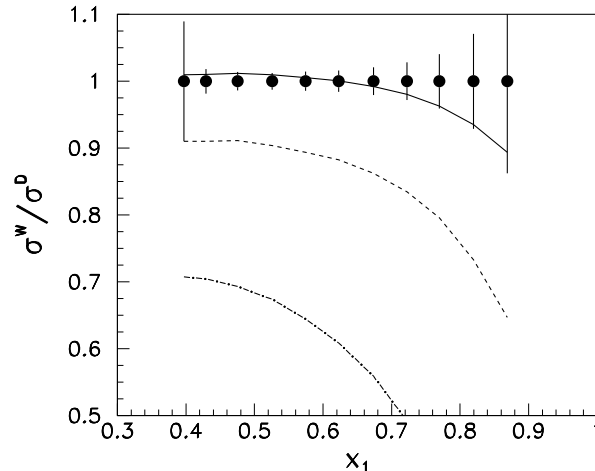


Figure 10: Expected statistical accuracy of E906 for the ratio of the Drell-Yan cross sections per nucleon for W/D vs. x_1 . Only events with $0.1 < x_2 < 0.2$ and effective mass above $4.2 \text{ GeV}/c^2$ have been considered. The systematic uncertainty in the cross section ratios is expected to be approximately 1%. The cross section ratios have arbitrarily been plotted at 1. The solid curve shows the expected cross section ratio for a fractional energy loss of 0.14%/fm (Eq. 10). The dashed curve shows the expected cross section ratio for a constant energy loss of 0.44 GeV/fm (Eq. 11), based on the procedures used to estimate path lengths in the E866 analysis [13]. The dot-dashed curve shows the expected cross section ratio for a constant energy loss of 2.73 GeV/fm, based on the procedures used to estimate path lengths in the reanalysis of E772 and E866 data [56].

theoretical motivation, but which nonetheless describe its observed x and Q^2 dependence quite well. But, as noted above, EKS98 also included E772 Drell-Yan data at $x_2 > 0.08$ in its fit. While most of the E866 statistics had x_2 well below this, there is a concern that some incident-quark energy loss may have been folded into the EKS98 shadowing fit inadvertently, thus obscuring the effect of energy loss during the E866 analysis. However, if the E866 data had been analyzed with a new shadowing parametrization that is based solely on DIS input data [59], rather than EKS98, the conclusions would have been similar to those in [13].

The best way to resolve this question is to perform a second Drell-Yan nuclear dependence study at a substantially lower beam energy. This amplifies the expected effect substantially, as seen in the $1/s$ dependence of Eqs. 11 and 12. Main Injector energies are ideal for such a study. One would like to observe the nuclear dependence of Drell-Yan scattering as a function of x_1 for moderate values of x_2 , where all models predict the cross section per nucleon should vary from nucleus to nucleus by no more than a few percent. The experiment will measure the x_1 dependence for those events that have $0.1 < x_2 < 0.2$. This x_2 region is comfortably above the traditional shadowing domain and below the momenta where the EMC effect and/or Fermi motion may modify the target antiquark densities. It was also investigated with moderate statistics by E772, providing a basis for comparison of events at comparable x_2 but quite different x_1 . Figure 10 shows the statistical accuracy that will be obtained for the Drell-Yan nuclear dependence as a function of x_1 during E906. The systematic uncertainty in the cross section ratios are expected to be approximately 1%. The cross section ratios in the figure have arbitrarily been set equal to 1. Only events which will satisfy the trigger and pass the target and dump cuts that have $0.1 < x_2 < 0.2$ and effective mass above 4.2 GeV have been included. Comparable statistics will be obtained for the cross section

ratios for the other two nuclear targets. To demonstrate the sensitivity of this measurement to incident-parton energy loss, the x_1 dependence that would expect for an energy loss equal to the upper limits found by E866 for models (10) and (11) above and for an energy loss equal to the result found from the “first-principles” reanalysis of E772 and E866 data has been calculated. The expected x_1 dependence of the cross section ratio per nucleon for W/D in model (12) is similar to that for model (11), but the two models will be distinguished by their different predicted A dependences. Overall, E906 will be a factor of 5 to 10 more sensitive to incident-parton energy loss than E772 or E866. The ultimate sensitivity will be limited by our ability to separate incident-parton energy loss effects from nuclear modifications of the target antiquark distributions, which will be determined largely by the results of the target antiquark studies that are also planned for E906.

2.5 Possible Future Measurements

This proposal focuses on measurements of Drell-Yan $\mu^+\mu^-$ production with the primary proton beam. A number of other interesting measurements could be made with this spectrometer, including Drell-Yan measurements with polarized protons on a polarized proton target to determine the spin structure of the sea distributions. When a polarized proton beam becomes available from the Main Injector, the present apparatus would be immediately suitable for that experiment. Even with an unpolarized beam there appear to be interesting correlations one can measure with Drell-Yan on a polarized proton target [60]. Intense secondary meson beams would open up new possibilities such as a more accurate determination of the charged kaon valence parton distributions or measurements of the ratio of d/u distributions of the proton as $x \rightarrow 1$.

While the production of the heavy $\bar{q}q$ pair from gluon-gluon fusion or quark-antiquark annihilations can be perturbatively calculated, the long-distance process involving the formation of the bound states is presently not amenable to calculation. Measurement of the polarization of produced quarkonia states can be used to understand the long-distance process. Fermilab E866/NuSea had made detailed measurement of J/ψ and Υ polarization [61]. A very interesting, complimentary measurement would be the polarization of the ψ' . A reconfiguration of the absorber wall (described in section 3.2) would allow for this study. In addition, with the reconfigured absorber, a study of the nuclear dependence of J/ψ production at lower beam energy could be done. The nuclear dependence of J/ψ and ψ' production was studied at 800 GeV/c in E866 [62] and at 200 GeV/c in NA3 [63]. The results appear to scale with x_F , but this could be examined with much higher statistical precision in the proposed detector than was achieved by NA3.

3 Experimental Apparatus

The design of the experimental apparatus leans heavily on the collective experience of E605, E772, E789 and E866 for the best technique to handle high luminosities in fixed target Drell-Yan experiments. The apparatus is optimized for events with large x_2 and $x_F \approx 0.2$. For scale, the muons generated by a 7 GeV virtual photon with $x_F = 0.2$ which decay perpendicular to the direction of motion (in the virtual photon rest frame) will in the laboratory have momenta of 33 GeV, an opening angle of 210 mr and transverse momenta of 3.5 GeV. A sketch of the apparatus showing trajectories for muons is shown in Figs. 11 (bend plane view) and 12. The key features of the apparatus are:

- Relatively short (<15% interaction length, L_I) targets to minimize secondary reactions in the target.

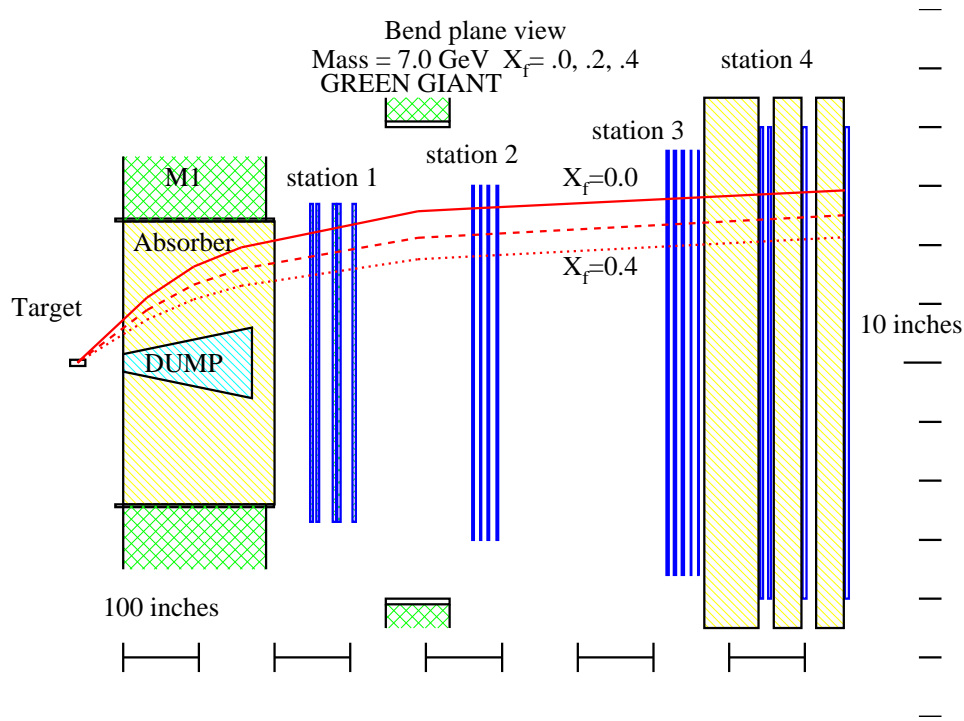


Figure 11: Bend plane view of the trajectories of one of the two muons resulting from the muonic decay of a 7 GeV virtual photon (which has x_F of 0.0, 0.2 or 0.4) in an 8 T-m spectrometer.

- Two independent magnetic field volumes, one to focus the high transverse momentum muons and defocus low transverse momentum muons and one to measure the muon momenta.
- A 15 L_I hadron absorber to remove high transverse momentum hadrons.
- A 30 L_I beam dump at the entrance of the first magnet.
- Zinc and concrete walls for muon identification at the rear of the apparatus (located after Station 3 and between the planes of Station 4).
- Maximum use of existing equipment consistent with the physics goals.

While the lower beam energy is a great advantage in terms of cross section and background rates and statistics, it has two disadvantages relative to 800 GeV/c experiments.

- The corresponding lower particle energies lead to increased probabilities for muonic decay of the produced hadrons. This is partially compensated by reducing the target-to-hadron-absorber distance to 1.3–1.8 m.
- The lower energy muons multiple scatter more easily in the hadron absorber.

As will be discussed below, the apparatus can be almost completely constructed by reusing or refabricating existing equipment. Only the first magnet requires a significant construction effort.

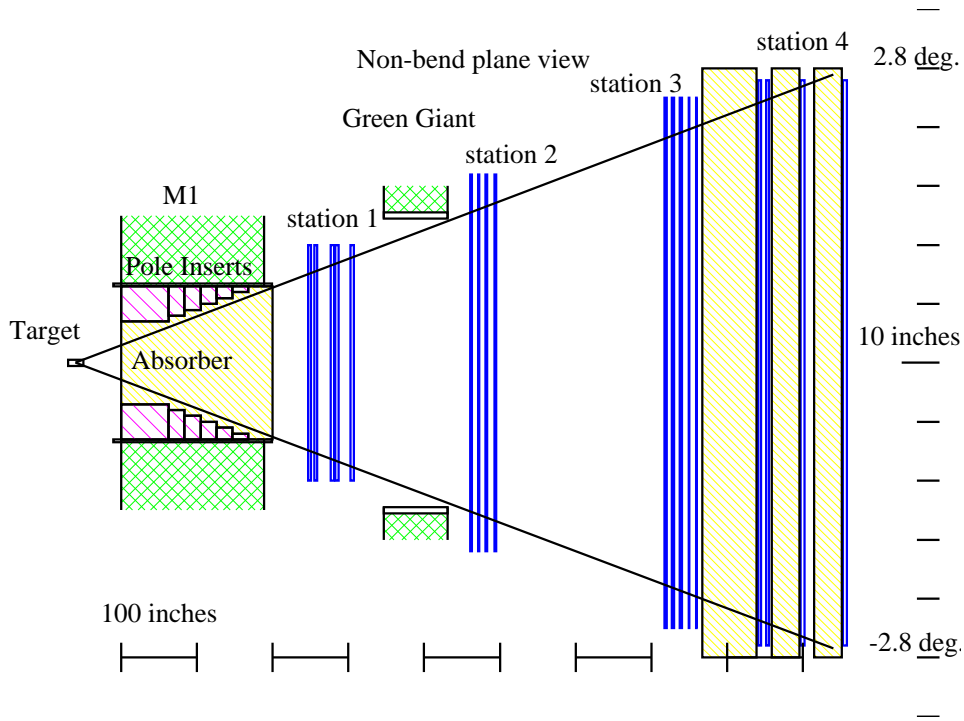


Figure 12: Non-bend plane view in an 8 T-m spectrometer. Only muons which pass around the beam dump in the bend plane contribute to the acceptance and so the beam dump is not shown.

3.1 Beam and Targets

The requirements for the beam are 10^{12} protons per pulse with a maximum beam spot size of 5 mm vertical by 10 mm horizontal and maximum divergence of 2 mr in each direction. The primary beam will stop in a 170" long trapezoidal copper beam dump starting with a 3" vertical height at $z=0$ extending to a 12" vertical height at $z=170$ ". Since the dump will absorb an average of 6400 watts of beam power, it will be water cooled with a closed loop recirculation system similar to the E866 beam dump.

The experiment would use 20" long liquid hydrogen and deuterium targets, three nuclear targets of approximately 10 gm/cm^2 thickness and a dummy liquid target cell. The targets would be remotely interchanged roughly every 30 minutes. The rapid Main Injector spill cycle will require blocking the beam for on the order of 30 sec to allow for target motion. The exact choice of nuclear targets has not been made but they are likely to be carbon, calcium or iron and tungsten. An advantage of iron would be a more direct comparison with the CCFR data. Tungsten would extend the nuclear dependence studies to a heavy nucleus, especially for the energy loss studies. Fermilab has been asked to provide the beam line instrumentation and suitable targets (either reusing the E866 targets or a new target system).

3.2 Magnets

The first magnet of the spectrometer focuses the high transverse momentum muons into the apparatus' acceptance and bends low momentum muons out of the acceptance. The optimal performance is obtained with a large aperture magnet [48" (y) by 26" (x)] whose transverse momentum, p_T , kick is approximately 2.5 GeV ($\approx 8.4 \text{ T-m}$). While reasonable Drell-Yan acceptance may be retained,

Table 1: The characteristics of the proposed M1 and the Jolly Green Giant magnet. The M1 horizontal aperture is without the pole inserts.

| Property | M1 | Jolly Green Giant |
|-------------------------|------------|-------------------|
| Length | 189 in | 84 in |
| Width | 95 in | 135 in |
| Height | 198 in | 190 in |
| Vertical Aperture | 48 in | 96 in |
| Horizontal Aperture | 26 in | 49.14 in |
| Field Integral | 8.14 T-m | 1.65 T-m |
| Ampere-Turns | 670230 | 101000 |
| Current | 2394 Amp | 980 Amp |
| Power | 0.58 MWatt | 0.89 MWatt |
| Inlet Water Temperature | 38°C | 35°C |
| Temperature Rise | 25°C | 22°C |
| Water Flow | 88 gal/min | 152 gal/min |
| Weight: | | |
| Pole Inserts | 9.5 t | |
| Coils | 19 t | |
| Return Yoke | 420 t | |
| Total | 450 t | 220 t |

provided the aperture of the downstream spectrometer is large enough, for lower field integrals, the singles rates dramatically increase to an unacceptable level. Even with the present design the experiment must be prepared for 100 MHz instantaneous rates in the first set of wire chambers.

The change in beam energy (boost) from from 800 GeV/c in E866 to 120 GeV/c in E906 means that the 570-inch “SM12” magnet used by E866 is not appropriate for this experiment. Instead, a new magnet must be constructed. An 189” long 8 T-m large aperture magnet can be constructed using 1/3 of the iron from SM12 and new coils, following the same general principles as the SM3 magnet. The characteristics of this magnet are given in table 1. Iron inserts will provide a tapered horizontal aperture of 98 mr opening angle tailored to the aperture of the second magnet. By using existing iron pieces for the return yoke, there should be minimal need to machine the radioactive iron. With such a magnet, there appear to be no experimental barriers to completing the measurement proposed here.

The second magnet must provide the accurate momentum determination with a large acceptance. The Jolly Green Giant (JGG) will be used for this purpose. The JGG is currently being used by Fermilab E907 (MIPP), but will be available for E906 when the experiment runs. The characteristics of the Jolly Green Giant are also given in table 1. For radiation protection purposes, the spectrometer, like the previous Meson-East spectrometer, will need to be vertically bending. The JGG is presently a horizontal bending (vertical field) magnet and will need to be remounted as a vertical bend magnet. Fermilab has been asked to undertake this reconfiguration.

The aperture around the beam dump in the first magnet will be filled with a graded hadron absorber. GEANT-based Monte Carlo’s are being used to optimize the configuration of the absorber. One possible configuration would be 80” of graphite, followed by 40” of copper then 40” of

Table 2: Wire Chamber Specifications and Singles Rates

| Station | Type | x size (cm) | y size (cm) | wire spacing (mm) | wire orientations | Number of Channels | Singles Rates (MHz) |
|---------|-------------|-------------|-------------|-------------------|-------------------|--------------------|---------------------|
| 1 | MWPC | 101.6 | 137.2 | 2.0 | Y,U,V,Y,Y',U',V' | 7000 | 40 |
| 2 | DC | 137.7 | 149.9 | 10.2 | Y,Y',U,U',V,V' | 1000 | 10 |
| 3 | DC | 203.0 | 162.4 | 20.3 | Y,Y',U,U',V,V' | 700 | 2 |
| 4 | Prop. Tubes | 254.0 | 211.0 | 10.0 | Y, Y', X, X' | 900 | 2 |

graphite and 40" of Borated Polyethylene. Al_2O_3 may be used in place of some of the Cu . The 40" of copper helps to eliminate particles which escape from the dump. The instantaneous single rates at each of the detector stations are given in table 2. The dominant single contribution is muons produced by the decays of hadrons in the dump.

The muons will lose approximately 3.5 GeV in energy passing through the absorber and multiple scatter by an average angle of $170/p_\mu$ mr (p_μ is the muon's momentum). This level of multiple scattering will still permit acceptable virtual photon mass resolution (approximately 240 MeV) and acceptable vertex resolution to separate target and beam dump events for muon energies greater than 15 GeV. Due to the long target length relative to the target-to-absorber distance, the target position provides minimal additional track constraints for the mass measurement.

3.3 Tracking Chambers

The possibly high instantaneous rates at station 1 lead require it to be able to handle rates up to 100 MHz. To handle these rates, Multi-Wire-Proportional-Chambers with a 2 mm wire spacing will be used. The first three planes would be MWPC's used in E605 with existing electronics. The stereo angles of the U and V wires are ± 14 degrees. The following four planes would use two existing E871 MWPC's, each covering half the x acceptance arranged with a 4" horizontal gap at $x = 0$. The frames of the two chambers would overlap in this gap. While multiple scattering in the frames does not significantly deteriorate the resolution, this $x = 0$ stripe avoids the highest count rate areas (at the maximum y). The stereo angle of these planes is ± 26 degrees. Existing E871 preamplifier-discriminator-readout would be used. Each of these wire chambers has 3 rf bucket hit resolution and would run with a fast gas (CF₄/isobutane, 80:20). The readout would consist of 7000 channels of coincidence registers. All the electronics and readout currently exist (E871 has 20000 wire chamber channels).

Stations 2 and 3 would use the existing E605/E772/E866 drift chamber stations 2 and 3. They are capable of 250 μ m resolution with Ar/Ethane (50:50) gas. The stereo angle is ± 14 degrees. Existing preamplifiers and discriminators would be adequate. Some of the electronic crates in which these components are mounted were replaced prior to E866's run in 1996. The remainder of the crates will need to be replaced. A 1700 channel multi-hit TDC system is required for good efficiency and rate capabilities. A more than sufficient number of LRS 3377 modules are expected to be available from the Fermilab PREP electronics pool [64].

Station 4 would be constructed of new, commercially available, limited streamer tubes with a 1 cm pitch operated in proportional mode, similar to those used by the PHENIX detector's endcap

muon id system. Existing amplifiers and discriminators from E866 will be used. The readout would be identical to the MWPC's and add 900 channels to the electronics and coincidence register total.

The rate dependence of the pattern recognition efficiency has been studied with Monte Carlo simulations to ensure that this choice of chamber configuration is acceptable. With 2.5 times the rates given in table 2, there is only a 4% decrease in efficiency, on the same scale as the level of rate dependent effects which were handled in E866.

3.4 Scintillator Hodoscopes

Scintillator hodoscope planes will provide the hit information for the hardware trigger system, just as they have in E866. Each of the four tracking station will have a y -measuring hodoscope plane associated with it. Each plane will have a total of 32 channels, separated into two groups of 16 channels for the left ($x > 0$) and right ($x < 0$) sides of the detector. There will be x hodoscope planes associated with detector stations 1 and 2, plus two additional planes as part of station 4. They will contain 32 channels apiece, separated into 16 channels for the lower half of the spectrometer ($y < 0$) and 16 channels for the upper half ($y > 0$). This segmentation will provide a logical division of each hodoscope plane into quadrants, allowing the trigger system to place tighter geometric constraints on the tracks than was done during E866.

All of the scintillators within a given y hodoscope plane will be the same size. The individual scintillators within hodoscope planes X4A and X4B will all be the same angular size. In contrast, the four X1 and four X2 scintillators closest to $x = 0$ will subtend half the angular range, and the scintillators furthest from $x = 0$ will subtend 1.5 times the angular range of the X4A and X4B scintillators and the remaining X1 and X2 scintillators. This segmentation minimizes the number of hodoscope channels in stations 1 and 2 that may be in coincidence with given channels in X4A and X4B, after accounting for the multiple scattering of the muons through the various absorbers in the spectrometer.

While many of the hodoscopes could be fabricated primarily by recutting and polishing the existing E866 scintillators to the sizes required for the new spectrometer, it is safer, given their age, to plan on constructing new scintillators and light guides for this experiment. The phototubes and bases from the existing E866 spectrometer will be reused (approximately 160 units). An additional 220 new phototubes and bases must be purchased to instrument the remaining channels. The existing E866 high voltage distribution systems will suffice to power the eight hodoscope planes.

For E866, the anode signals from each phototube were sent to LeCroy 4416 leading-edge discriminators. The discriminator outputs were reshaped by custom synchronizer/stretcher modules to provide clean, single RF bucket time resolution for all hodoscope planes except station 4, which had slightly worse than single bucket resolution. The higher background rates anticipated at the Main Injector due to the increased beam current make it very important to achieve clean, single RF bucket time resolution for all hodoscope planes. Given past experience, this should be straightforward with the existing discriminators for the hodoscopes in stations 1 and 2, and for the X4A and X4B planes. The longest scintillators in the spectrometer, those for Y4, will be only 7" shorter than the station 4 scintillators during E866 and phototubes will be placed on each end of these scintillators. With the double-ended readout and mean timers single bucket resolution will be achieved. Enough synchronizer/stretcher modules are available to instrument the entire new spectrometer.

3.5 Muon Identification

Final muon identification is provided with an absorber wall, 81 cm of concrete followed by 92 cm of zinc and 10 cm of lead, followed by 2 planes of streamer tubes and the X4A scintillators, then 92 cm of concrete followed by the Y4 and X4B scintillators and finally 92 cm of concrete followed by 2 planes of streamer tubes. The present E866 muon identification walls provide enough material for the smaller E906 wall [35].

3.6 Trigger

The hardware trigger system will examine the scintillator hodoscope hits to identify patterns characteristic of high mass muon pairs produced in the target. It will be conceptually similar to the system that was developed for E866 [65]. However, it will be enhanced substantially compared with the previous system, primarily to improve its ability to reject random coincidences that appear to form a candidate high p_T muon track. Such random coincidences represented over half of the apparent muon tracks observed during the E866 intermediate mass \bar{d}/\bar{u} running, and the background rates in the spectrometer due to soft muons are expected to be even higher at the Main Injector. The trigger modifications will also permit the implementation of two-dimensional masking of wire chamber hits during event analysis, based on the active hodoscope roads, which will reduce the combinatorics in the wire chamber track finding. Notably, this will minimize the frequency of hit-bank and track-bank overflows, one of the sources of rate-dependent reconstruction inefficiency that we encountered during E866. Finally, the trigger modifications will allow for the replacement of a number of custom CAMAC modules from the E866 trigger system that are now nearly 20 years old with new, more reliable and flexible units.

Electronically, the hardware trigger will consist of a single decision stage, implemented as a three-step parallel pipeline. In the first step, the outputs from the hodoscope synchronizer/stretcher modules will be routed to a set of logic modules similar to the LeCroy 2367 Logic Modules³. Eight modules will be dedicated to identifying four-fold Y1-Y2-Y3-Y4 coincidences characteristic of high p_T single muons produced in the target. Each time they observe a candidate track, they will output a bit indicating its charge, the side of the spectrometer (left or right) where it is located, the quadrant the track passed through at Y1, and the actual y location of the track at Y4. In general, Y1-Y2-Y4 triple coincidences would suffice since the spectrometer analyzing magnet is located between stations 1 and 2, and that is in fact how candidate tracks were identified during E866. Adding the extra constraint that the appropriate channel of Y3 must have a hit will help reject apparent tracks that actually consist of a random coincidence between hits in stations 1 and 2 due to one muon and a hit in station 4 due to another.

The \bar{d}/\bar{u} measurement will only be interested in a limited number of potential track roads through the spectrometer. However, the eight LeCroy 2367 modules required to identify all of those tracks contain enough additional internal logic and I/O capability to cover the entire phase space of four-fold Y1-Y2-Y3-Y4 coincidences associated with real tracks originating from either the target or the beam dump. This will provide maximal flexibility when designing triggers for study purposes or ancillary measurements.

Four additional LeCroy 2367 modules will be dedicated to identifying candidate tracks originating from the target that include coincidences among at least three of the four planes X1-X2-X4A-X4B. Each time they observe a candidate track, they will output a bit indicating the side of the spectrometer where it is located, the quadrant the track passed through at X1 and X2, and

³Note that if LeCroy 2367 Modules are no longer available, a custom fabricated electronics solution can easily be found.

the actual x location of the track at X4A and X4B. This represents a significant upgrading of the tracking capability of the hardware trigger in the x direction, compared with E866, and will permit full two-dimensional constraints on the tracks. It will also make continuous monitoring of the efficiency of the y hodoscopes practical. This will be important because the ability to average over long-term variations in the spectrometer efficiency between targets will be reduced at the Main Injector, since it will be difficult to change amongst the various targets as frequently as was done during E866. In contrast, for E866 special hodoscope efficiency studies were run every few weeks. They consisted of a series of runs utilizing a special trigger configuration, sequentially turning off the high voltage on sets of x hodoscopes near the center of the spectrometer.

The second step in the trigger pipeline will combine the x and y tracking results from the first step to identify events with candidate high p_T muons present. This will be done in a pair of LeCroy 2367 modules, one dedicated to tracks on the left side of the spectrometer and one dedicated to tracks on the right side. The candidate muons will be characterized according to their charge, the side of the spectrometer on which they are located, and a rough measure of their p_T . Events will also be tagged that appear to have two muons with opposite charges present on the same side of the spectrometer.

In parallel with the first two steps of the main trigger sequence, OR's of all the scintillators on each side of each plane will be generated and routed to a Track Correlator [65] to generate simple cosmic ray and noise triggers for diagnostic purposes. This procedure was utilized during E866, and the same CAMAC and NIM electronics will be reused at the Main Injector.

The final step in the trigger pipeline will generate the actual triggers, handle the experiment busy logic, and strobe the read-out electronics. This step will either be performed with one additional LeCroy 2367 module or with the Track Correlators and Master Trigger OR that were designed and constructed for the E866 hardware trigger [65]. The primary physics trigger will consist of a coincidence between two candidate $x - y$ tracks of opposite charges, on either the same or opposite sides of the spectrometer. If the background trigger rate due to low mass muon pairs is higher than desirable, a rough measurement of the p_T for the two muons from the previous step may be added to provide a crude effective mass cut on the muon pair in hardware. A similar procedure, but with less granularity than anticipated with the new trigger system, was adopted for several of the data sets taken during E866. It reduced the raw trigger rate during the E866 intermediate mass \bar{d}/\bar{u} data taking by a factor of three, with essentially no reduction in efficiency for the Drell-Yan muon pairs of interest. Two triggers will be used to determine the rate of random coincidences between two muon tracks in the same RF bucket, both of which originate from the target and, thus, are indistinguishable from a real Drell-Yan muon pair. One of these triggers will record events that contain two muons of the same charge when they are located on opposite sides of the spectrometer, while the other will record a prescaled set of single-muon events. E866 has demonstrated that an excellent simulation of the random coincidence background can be obtained by combining muons from single-muon triggers into pairs, then normalizing their number to the observed rate of like-sign coincidences. Two additional triggers will select prescaled samples of events that contain a candidate track in either the x or y direction, but not necessarily both. The events with x tracks will be used to monitor the absolute efficiencies of the y hodoscopes, and the events with y tracks will be used to monitor the absolute efficiencies of the x hodoscopes. The last trigger will provide a luminosity-weighted read-out of all detector elements during random RF buckets, independent of the status of any of the spectrometer hodoscopes. This will be used to provide an unbiased measure of the background occupancy rates throughout the spectrometer, which are very important for estimating rate-dependent reconstruction inefficiencies.

3.7 Monte Carlo of Trigger and Spectrometer Rates

Thorough Monte Carlo simulations have been done to determine both the detector response and resolution, and spectrometer and trigger rates. Two different Monte Carlo codes have been used for these simulations. The primary one is a modified version of the “Fast Monte Carlo” that was originally written to estimate acceptances in E605/E772/E789/E866. It has now been modified to simulate the detector configuration for this proposal, E906. This Monte Carlo simulates muons from Drell-Yan, resonance production (J/ψ , ψ' , Υ , $\Upsilon(2S)$, $\Upsilon(3S)$), and π , K and charmed meson decays. It can track single muons or pairs through the entire spectrometer in order to estimate signal and background rates with realistic hardware trigger simulation. It also simulates the traceback of the muon tracks to the target so that realistic tracking cuts may be imposed and the ultimate resolutions of the spectrometer can be estimated. The details of the thrown spectra and assumed cross sections can be found elsewhere [66]. The second code is a GEANT-based Monte Carlo. This code was written to optimize the design of the hadron absorber wall. Unlike the first code, this Monte Carlo only tracks particles as far as Station 1. However, it tracks all particles which arise from proton interactions in the targets and beam dumps, rather than just muons, so it is quite useful for configuring the hadron absorber that will fill the aperture of the large M1 magnet. Both codes have been demonstrated to give a reasonable description of the rates that were observed during E866, and they give consistent results for the flux of muons with momenta above 3 GeV/ c that should be present in Station 1 at the Main Injector.

The Fast Monte Carlo code has been verified through a number of further tests. For E906, its prediction of the flux of muons with momenta above 3 GeV/ c that should be present at Station 1 is consistent with a full GEANT simulation of the target, beam dump, magnet and absorbers. The simplified muon traceback to the target has been checked by verifying that it reproduces observed resolutions during E866. For example, the predicted and observed J/ψ mass resolutions during the E866 large- x_F nuclear dependence study agree to within 10%.

The Monte Carlo has been used to estimate the trigger rates. The rates of muon pairs from Drell-Yan and resonance production originating in either the target or the dump have been simulated for the equivalent of 10^3 to 10^5 spills at an assumed intensity of 10^{12} protons per 1 s spill. (The Main Injector cycle time provides for a 1 s spill every 2.9 s [67].) The rate due to Drell-Yan pairs off the LH_2 target is 0.55/spill, with approximately half of these passing the tracking and effective mass cuts. The total real⁴ rate is expected to be approximately 90 events/spill, with approximately 15% of these passing trigger matrix cuts, depending on the target. The vast majority of the events are from J/ψ 's produced in the beam dump and do not pass trigger requirements. Of the triggered events, approximately two thirds originate from Drell-Yan pairs produced in the beam dump. The yield of muon pairs from $D\bar{D}$ production is very small. At $\sqrt{s} = 15$ GeV, there will be very few Υ events ($m_\Upsilon = 9.5$ GeV/ c^2) over the life of the experiment. These rates are summarized in Tab. 3.

In addition to the real pairs, there will be a significant number of triggers from random coincidences of two independent muon tracks. When running with the liquid hydrogen target, the primary source of background single muons will be π and K decay-in-flight in the beam dump. When running with the liquid deuterium target, the π and K decay-in-flight background from the target will be slightly larger than that from the dump. The total rate of single muons traversing the detector and passing the trigger matrix tracking will be approximately 48 kHz with the LH_2 target and 71 kHz with the LD_2 target. In each case, the Monte Carlo predicts that the ratio of positive to negative muons will be approximately 2:1, as shown in Tab. 4. To obtain a conservative estimate of the trigger rate, the predicted rates of true single muon triggers have been doubled in

⁴Here, “real” refers to those oppositely signed muon pairs from the same event, such as Drell-Yan or J/ψ decay, as opposed to random coincidences of single muons.

Table 3: Expected rate of events which traverse the detector and trigger rates per 1 s spill of 10^{12} protons from real and random coincidences with liquid hydrogen and deuterium targets and the copper beam dump. The ratio of deuterium to hydrogen rates reflects the difference in the densities of liquid deuterium and hydrogen. Note that the random coincidences for each target include contributions from the beam dump.

| | LH_2 | | LD_2 | | Copper Beam Dump | |
|--|----------|--------------|--------|---------------|---------------------|----------|
| | Evt.s. | Trig. | Evt.s. | Trig. | Evt.s. | Trig. |
| Drell-Yan ($m_\gamma > 3 \text{ GeV}/c^2$) | 0.55 | 0.35 | 1.47 | 0.93 | 17.6 | 7.8 |
| $J/\psi, \psi'$ | 2.53 | 0.23 | 6.03 | 0.56 | 72.0 | 3.4 |
| $\bar{D}D$ | > 0.01 | > 0.01 | 0.01 | > 0.01 | 0.11 | > 0.01 |
| random coincidences | | ≈ 50 | | ≈ 100 | | - |

Table 4: Expected single muon rates per 1 s spill of 10^{12} protons from decay-in-flight mesons which pass through the detector (μ 's) and satisfy trigger matrix tracking requirements (Trks.) from liquid hydrogen and deuterium targets and the copper beam dump.

| | LH_2 Target | | LD_2 Target | | Copper Beam Dump | |
|-------------------------|------------------|--------|------------------|--------|---------------------|--------|
| | μ 's | Trks. | μ 's | Trks. | μ 's | Trks. |
| π^+ decay-in-flight | 40.6 k | 6.1 k | 97.7 k | 14.6 k | 75.9 k | 6.5 k |
| π^- decay-in-flight | 17.4 k | 4.1 k | 41.9 k | 9.8 k | 38.2 k | 10.1 k |
| K^+ decay-in-flight | 31.5 k | 6.5 k | 75.8 k | 15.6 k | 69.6 k | 10.3 k |
| K^- decay-in-flight | 3.1 k | 1.3 k | 7.6 k | 3.1 k | 8.8 k | 4.2 k |
| Total μ^+ | 72.1 k | 12.6 k | 173.5 k | 30.2 k | 145.5 k | 16.8 k |
| Total μ^- | 20.5 k | 5.4 k | 49.5 k | 12.9 k | 47.0 k | 14.3 k |

order to account for random contributions to the single muon rate and finite duty-factor of the proton beam when estimating the random pair rates. Using a time resolution equivalent to the Main Injector clock frequency of 53 MHz, this leads to estimates of 50 random dimuon triggers per spill for the LH_2 target and 100 random triggers per spill for the LD_2 target, counting all random opposite-sign pairs and the random like-sign pairs that have one muon on each side of the spectrometer. These random trigger rates do not include the additional suppression that will be obtained by constraining the apparent mass of the pair in hardware. Experience from E866/NuSea indicated that these random pairs will have a mass spectrum strongly peaked at masses near or below the J/ψ .

Approximately 80 study triggers per spill will be taken, including prescaled single muons to study the random background, triggers to monitor the efficiency of the hodoscopes, and triggers to investigate any rate-dependence that may be present in the data analysis. Therefore, an overall rate of approximately 200 triggers or less per spill is expected. For planning, a trigger rate of 1 kHz is assumed. With full analysis cuts, the real to random rate is expected to be 5 to 1 at all x_2 values, and much better than that at large x_2 .

Most of the background triggers are eliminated in the analysis by simple cuts based whether the

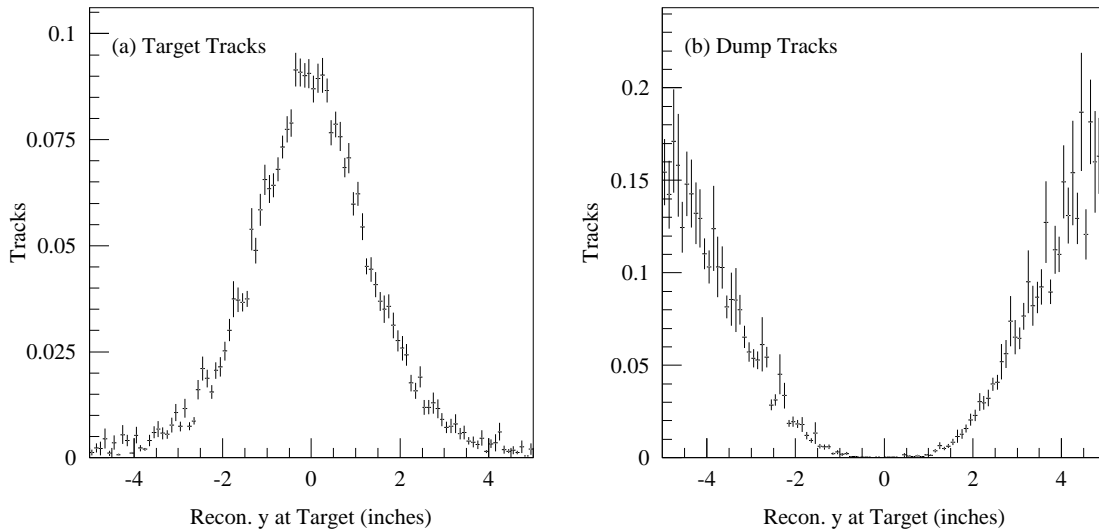


Figure 13: Distance in y of reconstructed track from target center for (a) Drell-Yan and ψ events produced in the target and (b) Drell-Yan and ψ events produced in the dump. To be considered as an event from the target, *both* tracks must reconstruct within 2.25 inches of $y = 0$.

track points back to the target and the track's proximity to the beam dump. Histograms of these quantities are shown in Figs. 13 and 14, respectively. An accepted track needed to pass within 5.7 cm of the target in y and be at least 5.7 cm in away from $y = 0$ cm at the front face of the beam dump. Clearly these restrictions will remove the vast majority of unwanted tracks. In addition, to remove contamination from the ψ and Υ resonance families, the mass of reconstructed muon pair must be between $4.2 \text{ GeV}/c^2$ and $8.8 \text{ GeV}/c^2$.

In addition to trigger and spectrometer rates, the Monte Carlo was also used to estimate the expected resolution of the detector. For simulated Drell-Yan events which pass the trigger and reconstruction cuts, the expected mass resolution is $\sigma_m = 0.2 \text{ GeV}/c^2$ and the x_2 resolution is $\sigma_{x_2} = 0.02$. These are shown in Fig. 15.

3.8 Data Acquisition System

In order to achieve the goals put forward in this proposal, the data acquisition system must be able to: (1) digitize and move to tape detector hits from MWPC's, hodoscopes, streamer tubes and drift chambers at trigger rates of up to 1 kHz with very small dead time; (2) include information on the trigger condition in the data stream; (3) provide for on-line monitoring of detector efficiencies and the status of main system components; (4) provide for control of experimental systems such as moving targets and programming trigger modules. All of these capabilities were available in the DAQ system which was used for Fermilab experiment E866. However, several features of the E866 system must be changed to accommodate the Main Injector experiment.

The readout system for E866 used the TRANSPORT interface, which was built by the NEVIS electronics group in 1980, to hoist data from custom built TDC's and coincidence registers to tape. Many problems were encountered with that system during the startup of E866, and intermittent problems during data acquisition. Both the age of the system and the constraints that it imposes on the data stream require that it be replaced for the new experiment. Because they are to operate

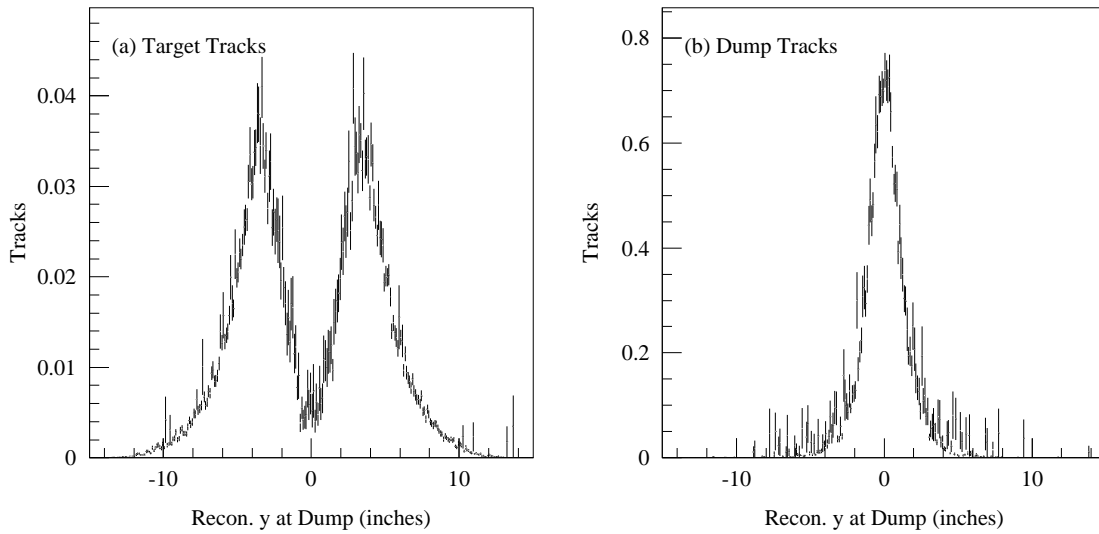


Figure 14: Distance in y of reconstructed track from the beam dump center at the face of the dump for (a) Drell-Yan and ψ events produced in the target and (b) Drell-Yan and ψ events produced in the dump. To be considered as an event from the target, *both* tracks must reconstruct at least 2.25 inches away from $y = 0$ at the dump.

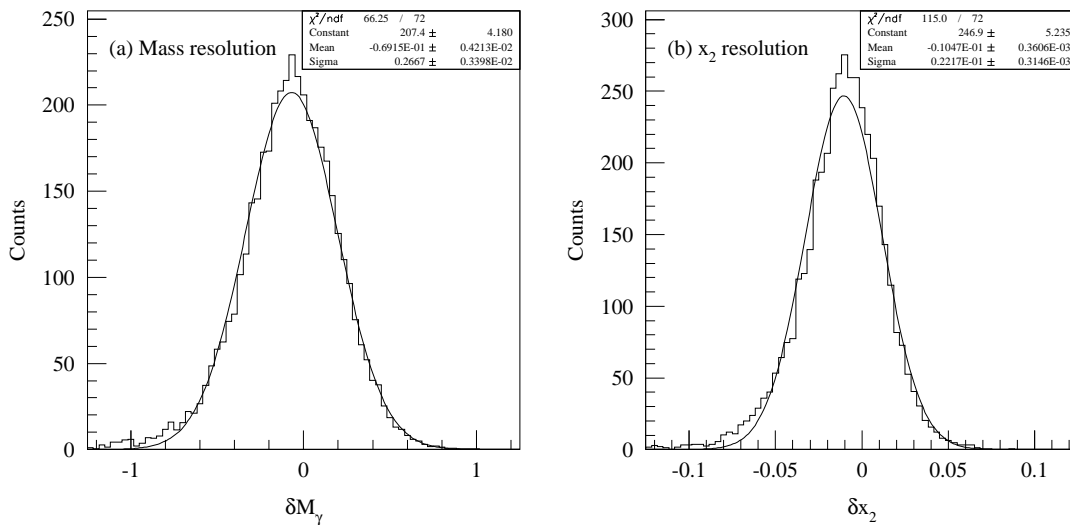


Figure 15: Expected (a) mass and (b) x_2 resolution for accepted Drell-Yan event using the proposed detector.

in a high rate environment, the drift chambers will need to be read out with multi-hit TDC's which precludes using the TDC's from the E866 readout system.

Most of readout requirements for the proposed experiment can be met by the front end system that has been assembled for Fermilab experiment E871, which, while it will be 10 years old when E906 runs, is available for use by E906 [68]. The E871 system will provide a high speed readout path for the MWPC's, hodoscopes and proportional tubes configured here. Multi-hit TDC's and the appropriate interface connection to the Processor Bus to read out the drift chambers will be added.

The computer architecture used in E871 is very similar to that planned for this project. Our trigger rates, however, will be much lower than those for E871 and event lengths will be comparable so the dead time using their system should be extremely small. As in E871, data will be moved from front end modules to buffer memory and then written out on tape units. One tape unit should suffice to handle the anticipated bandwidth with average event lengths of less than 1.5 kB and trigger rates less than 1 kHz. Event sampling will be done to monitor wire chamber and hodoscope efficiencies using UNIX based workstations or PC's running LINUX.

The DAQ system for this project will follow DART standards and use DART software. This represents another break from the E866 system which did not use DART. The E871 DAQ system uses DART so the front end readout is already compliant with DART standards. With the exception of trigger programming, the remaining system requirements for the new experiment proposed here are already available in DART software packages.

3.9 Analysis

The analysis of the data accumulated in these measurements should be straightforward, both in offline production and for online monitoring. The analysis will be similar to that done for E866 and would employ farms of LINUX PC's. An estimate of the scope of the analysis task can be made from the expected trigger rate of 1 kHz (1/3 kHz average), estimated event size of 1.5 kB, and a compute time per event of 20 ms/event (on an 180 MHz HP PA8000) based on analysis of data in E866/NuSea. Scaling with floating point performance to a 1 GHz Pentium III (a current "commodity" PC) three of these Pentium CPU's can analyze the data as fast as it would be taken. In the counting house we generally want to be able to fully analyze about 10 to 20% of the data as it is accumulated and this could be accomplished with only one or two of these PC's. Naturally, since the typical CPU power per dollar increases by perhaps a factor of two per year, by the time this experiment would actually run the hardware available would even more easily address these analysis problems.

The typical taping rate is estimated to be about 0.5 MB/s (easily within the bandwidth of present Digital Linear Tape (DLT) technology) and would result in about 43 GB of data on tape per day, or about 5 TB for the entire run. To analyze these data as fast as they were taken means the networks that support distribution of the data would need to transport in excess of 0.5 MB/s, easily within the capability of 100 base-T networks.

Since the planned detector system would be conceptually similar to that used in E866, the analysis algorithms from E866 should be applicable to the new experiment. Therefore, much of the old code will be reused. Since much of the raw data format will probably be new the data unpacking parts of the code would probably be rewritten in C or C++, while other parts that need not change may remain in FORTRAN. Since the code already runs on the Fermilab UNIX farms using the Fermilab parallel processing environment (CPS), it should be straightforward to preserve that capability. CPS is already ported and being used on LINUX PC farms at Fermilab.

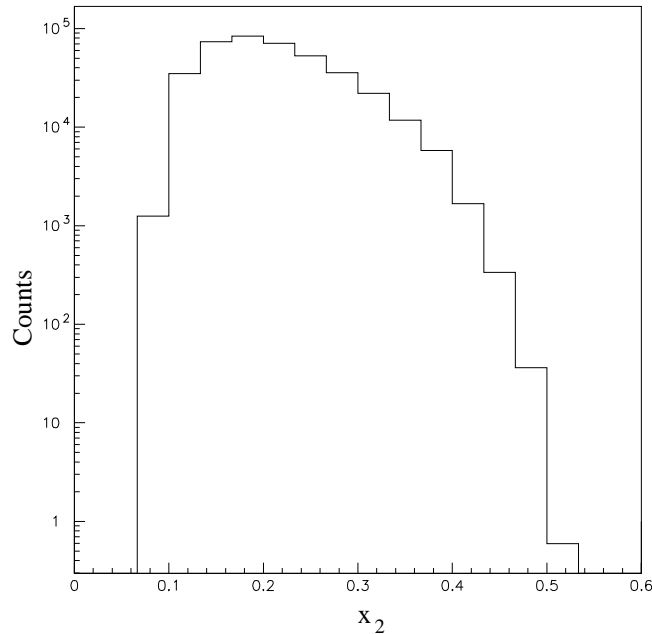


Figure 16: Monte Carlo results for yields from a 90 day 50% efficiency run with 10^{12} protons per pulse on a 20" long liquid hydrogen target with the apparatus shown in Figs. 11 and 12. This represents all accepted events with masses between 4.2 and 8.5 GeV/c^2 with $x_F > -0.1$. The number of counts will be the same on the nuclear targets and 70% greater on deuterium.

3.10 Yields

Figure 16 shows the results from a Monte Carlo simulation of the expected yields of this spectrometer for a hydrogen target in 90 days at 50% efficiency running. With an 9 month run at 50% total efficiency (66% accelerator, 75% experiment), these yields would be reached on 5 targets (hydrogen, deuterium and three nuclear targets, relative running time: 35% H, 26% D, 35% nuclear, 4% Dummy liquid cell) and achieve the relative errors on the ratio of the deuterium to hydrogen cross sections for $x_F > -0.1$ shown in Fig. 2. E866 was able to maintain systematic errors on the cross section ratio to better than 1%, and it is anticipated that E906 will also be able to achieve 1% systematic errors in the ratio. With these yields, the statistical precision of the extraction of \bar{d}/\bar{u} is shown in Fig. 17 relative to the expectation with MRST parton distributions.

4 Costs and Schedule

A construction timetable for the new magnet and apparatus has been developed that will allow the experiment's construction to be completed in August 2007. Coil fabrication and assembly of the new magnet is estimated to take 21 months from the beginning of design work through installation, including 2.5 months of "contingency" time. Following this, three months have been allocated to map the magnet and configure the hadron absorber within its aperture. Once these operations are completed, 2.5 months have been allocated to move the the JGG magnet into position (configured as a vertical bending magnet) and mapped its field. The preparation tracking and hodoscope stations will take place in parallel with magnet construction. After the installation and mapping of the magnets is completed, the more delicate tracking and hodoscope stations will be mounted

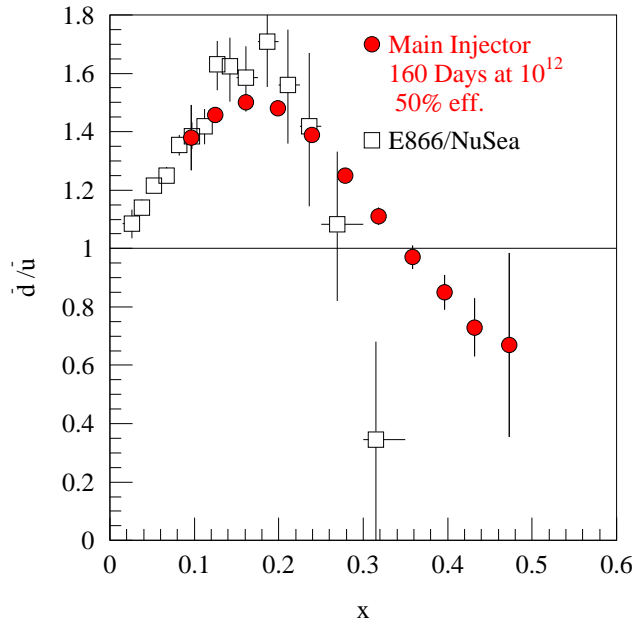


Figure 17: Projected results for the extraction of \bar{d}/\bar{u} from a 160 day 50% efficiency run with 10^{12} protons per pulse on a 50 cm long liquid hydrogen and deuterium targets with the apparatus shown in Figs. 11 and 12 based on the MRST [5] distribution of \bar{d}/\bar{u} . Also shown are the E866/NuSea results [11].

in the detector. Eight months have been allocated for this installation and other tasks related to pre-beam commissioning of the apparatus. The construction timeline is shown in Fig. 18.

This schedule would allow for a start date for the experiment of January 2008, which will mesh well with the expected Fermilab schedule. Fermilab plans to run E906 at the same time it runs E921/CKM [14]. Because of “proton economics”, it is very unlikely that this will happen while the MINOS experiment is running. MINOS forecasts reaching “CD-4 Start of Operations” on 11 January 2005 [69] and 3 years of running after that. E906 should be ready several months before this because low intensity proton beams could be available to commission the detector. This would then allow for optimal use of the high intensity beam in January 2008 with a fully tested apparatus.

In order to maintain this schedule, funding for magnet design must begin in FY2005. In addition, the design work on the trigger electronics should begin in FY2005. The magnet’s aluminum conductor and insulator may also be purchased in that year. The bulk of the costs in FY2006 involve the fabrication of the magnet’s coils and the assembly of the magnet. In addition, work must begin on some of the detector systems in FY2006. In FY2007, major equipment items include the purchase of photomultiplier tubes for the hodoscopes, the purchase of Station 4 prop. tubes and the fabrication of the trigger electronics. The complete funding profile is shown in Tab. 5. In FY2005, \$602,000 is requested, followed by \$1,337,000 in FY2006 and \$624,000 in FY2007. The funding request broken down by institute is shown in Tab. 6.

The largest new element of the spectrometer is the muon focusing magnet. It will be constructed following the same design principles as the SM12 and SM3 magnets⁵. The magnet is designed to reuse whole pieces of the SM12 iron flux return yoke with minimal additional machine work, and

⁵The SM12 magnet from Fermilab E866 is being replaced by this magnet, the SM3 magnet is being replaced by the JGG

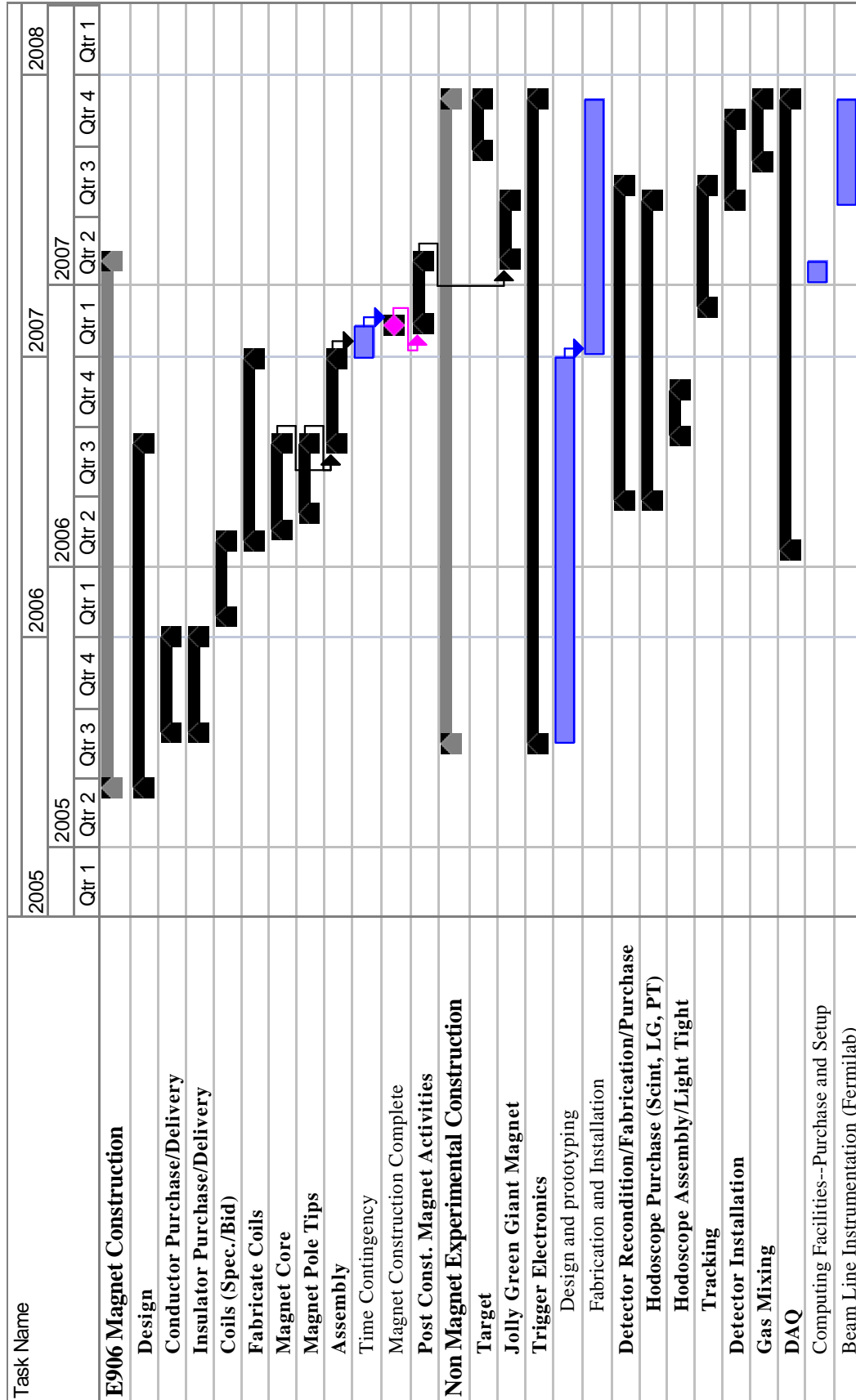


Figure 18: Gantt chart for completion of the E906 spectrometer magnet and detector.

Table 5: The required funding profile for the construction of the focusing magnet and detector equipment for Fermilab E906, by fiscal year and task, rounded to the nearest \$1,000. The “Base Cost” is in 2002 dollars, unless noted and is exclusive of contingency and overhead. All other costs include contingency, overhead and escalation at the rates listed.

| Task | Institute | Base Cost | Contingency | Overhead | Escalation | FY2005 | FY2006 | FY2007 | Total |
|-----------------------------|-----------|-----------|-------------|----------|------------|---------|-----------|--------|-----------|
| Magnet Design | Argonne | 153,000 | 15% | 26.4% | 1.076 | 240,000 | | | 240,000 |
| Aluminum Conductor | Argonne | 142,000 | 15% | 10.0% | 1.076 | 194,000 | | | 194,000 |
| Insulator | Argonne | 83,000 | 15% | 10.0% | 1.076 | 113,000 | | | 113,000 |
| Coil—Tooling Design & Fabr. | Argonne | 193,000 | 15% | 10.0% | 1.076 | | 263,000 | | 263,000 |
| Coil—Fabr. Setup & Staging | Argonne | 63,000 | 15% | 10.0% | 1.106 | | 88,000 | | 88,000 |
| Coil—Fittings and Parts | Argonne | 27,000 | 15% | 10.0% | 1.106 | | 38,000 | | 38,000 |
| Coil—Fabr. | Argonne | 590,000 | 15% | 10.0% | 1.106 | | 826,000 | | 826,000 |
| Coil—Shipping to Fermilab | Argonne | 31,000 | 15% | 10.0% | 1.106 | | 43,000 | | 43,000 |
| Mag. Core & Assembly Parts | Argonne | 60,000 | 15% | 10.0% | 1.106 | | 84,000 | | 84,000 |
| Magnet Pole Tips | Argonne | 45,000 | 15% | 10.0% | 1.106 | | 64,000 | | 64,000 |
| Absorber Purchase Al_2O_3 | Argonne | 2,000 | 25% | 10.0% | 1.106 | | | 2,000 | 2,000 |
| Magnet Construction Total | | 1,389,000 | | | | 547,000 | 1,406,000 | 2,000 | 1,955,000 |

| Task | Institute | Base Cost | Contingency | Overhead | Escalation | FY2005 | FY2006 | FY2007 | Total |
|------------------------------|------------|------------------------|-------------|----------|--------------------|---------|-----------|---------|-----------|
| Trigger Electronics | Texas A&M | 95,000 | 25% | 26.4% | 1.076 | 54,000 | | 89,000 | 143,000 |
| Hodos.—Scint. & Light Guides | Abilene | 91,000 ^a | 15% | 0.0% | 1.028 ^a | | 108,000 | | 108,000 |
| Hodos.—Phototubes | Abilene | 138,000 | 15% | 0.0% | 1.135 | | | 179,000 | 179,000 |
| Tracking—Electronics Crates | Rutgers | 6,000 | 15% | 0.0% | 1.135 | | | 8,000 | 8,000 |
| Tracking—Station 4 | Los Alamos | 104,000 ^b | 20% | 0.0% | 1.457 ^b | | | 182,000 | 182,000 |
| Tracking—Gas Mixing Sys. | Argonne | 25,000 | 15% | 10.0% | 1.135 | | | 36,000 | 36,000 |
| Data Acquisition | Argonne | 35,000 | 15% | 10.0% | 1.041 | | 46,000 | | 46,000 |
| Counting House Computing | Argonne | 15,000 | 15% | 10.0% | 1.041 | | | 20,000 | 20,000 |
| Detector Construction Total | | 533,000 ^c | | | | 54,000 | 154,000 | 514,000 | 722,000 |
| E906 Total Cost | | 1,922,000 ^c | | | | 601,000 | 1,560,000 | 516,000 | 2,677,000 |

^aVendor’s estimate included 3%/year inflation through 2005. Base cost for the scintillator is \$63,000 and for the light guides is \$20,000 in 2002 dollars.

^bFrom 1992 PHENIX estimate so that escalation is figured from 1992. The base amount is \$135,000 in 2002 dollars.

^cBase cost is given in 2002 dollars.

Table 6: Experimental equipment budget broken down by institute and fiscal year.

| Institute | FY2005 | FY2006 | FY2007 | Total |
|------------|---------|-----------|---------|-----------|
| Argonne | 547,000 | 1,452,000 | 58,000 | 2,057,000 |
| Texas A&M | 54,000 | | 89,000 | 143,000 |
| Abilene | | 108,000 | 179,000 | 287,000 |
| Rutgers | | | 6,000 | 6,000 |
| Los Alamos | | | 182,000 | 182,000 |

Fermilab has reserved sufficient iron from SM12 for the new magnet. Several different methods to produce the magnet coils were evaluated on the basis of total cost to the project. These designs included construction based on welding straight and bent copper sections, a similar design with aluminum sections and a design which used long aluminum conductor from large reels which were then bent into the appropriate coil shape. The latter option of winding the coils from 1.6 inch square hollow aluminum conductor on large reels was chosen because of its lower overall cost.

The cost of producing the new magnet is given in Tab. 5. These are based on a detailed estimate done at Argonne [70], and include:

Magnet Design: The design will be done by the APS division at Argonne and will take roughly 8.5 Physicist/Engineer months at \$11,745/month and 7 Designer months at \$7,662/month.

Aluminum Conductor: The coils will be made from aluminum alloy 1350 conductor. Supplied on 700 foot reels, the conductor will cost \$142,000, including the cost of the metal (\$34,000), tooling and dies for extruding the aluminum (\$3,000), the reels themselves (\$5,000), fabrication costs (\$96,000), shipping (\$2,000) and testing (\$2,000).

Insulator: The conductor will be insulated with a two layer wrap of Scotchply and Rex-i-flex followed by ground wrap layers of Scotchply and Rez-i-flex around the individual coil “pancakes”. A somewhat higher contingency of 30% has been allocated to these supplies because of some uncertainties about its availability in future years.

Coil—Tooling Design and Fabrication: The major tooling costs for coil manufacturing include the insulator curing molds (\$111,000), winding fixture (\$31,000), lifting fixture (\$15,000) and other, smaller cost items (totaling \$21,000).

Coil—Fabrication Setup and Staging: The time required by the coil vendor to for setting up the above tooling and the staging for the coil fabrication. This was figured for 1500 hrs at \$42/hr.

Coil—Fittings and Parts: This category include all of the miscellaneous sleeves, center taps, flags, jumpers, water fittings, manifolds, etc which are needed for the coils.

Coil—Fabrication: Detailed estimates of the labor for coil fabrication have been done [70]. It is estimated that coil fabrication will require approximately 12,500 hrs of technician time at \$45.80/hr and 270 hrs of machinist-welder-rigger time at \$81.18/hr.

Coil—Shipping to Fermilab: This cost is based on six shipments at \$3645 and five return shipments of the fixtures/shipping frames at \$1735. This cost will, of course vary depending on where the vendor fabricating the coils is located.

Magnet Core and Assembly Parts: To wind the aluminum conductor into “pancakes” is estimated to require 320 hrs of technician time at \$45.80/hr and 8 hrs of machinist-welder-rigger time at \$81.18/hr for each of the 14 pancakes.

Magnet Pole Tips: Geometrical constraints show that 16,100 lbs of steel are needed for the magnet’s pole pieces. The cost was based on an estimate of \$2.75/lb for machined steel.

Fermilab has been requested to handle the assembly of the new magnet. This cost is not included in this grant request.

The trigger electronics, scintillator hodoscopes and photomultiplier tubes, and station 4 proportional tubes represent the other major costs to the experiment. These costs include:

Trigger Electronics: The trigger electronics are based on LeCroy 2367 Logic Modules, which were used in E866. Fifteen of these units are needed, however they are no longer available from LeCroy. A total of \$141,000 is needed, based on the actual cost of the LeCroy units, if they were available, plus associated hardware and software for development. These numbers include a 25% contingency. Roughly \$54,000 is needed in FY2005 for development and the remaining \$88,000 in FY2007. The Texas A&M is responsible for the development and fabrication of the trigger.

Hodoscopes—Scintillator, Light Guides, Phototubes and Misc. Supplies: The scintillator for the new hodoscopes will cost \$81,000 with an additional \$25,000 for light guide material, based on a quote by the Ludlum Corporation. The hodoscope array will need 384 photomultiplier tubes. Of these approximately 160 will be reused from E866 leaving an additional 220 tubes, bases and shields to be purchased at an estimated cost of \$179,000, based on estimates from Electron Tubes (formerly Throne-EMI). The scintillators and light guides will be purchased in FY2006. The purchase of the photomultipliers will be delayed until FY2007 to help maintain a more level budget. The hodoscope arrays are the responsibility of Abilene Christian University. In total the new hodoscope array will cost \$287,000, which includes 15% contingency.

Tracking—Electronics Crates: Some of the electronics crates for Stations 2 and 3 were replaced prior to the running of E866 in 1996. The remainder date from even earlier experiments, and these, older crates have questionable reliability and should be replaced.

Tracking—Station 4: The station 4 proportional tubes will be similar to those used by the PHENIX muon-id system, which used commercially available detectors. The cost for the PHENIX muon-id system, including electronics, was estimated at roughly \$140 per channel in 1993. Scaling this to the number of channels required by E906 and taking into account inflation, roughly \$182,000 is required. Contingency of 20% is included with these numbers. The Los Alamos P-25 group is in charge of the station 4 proportional tubes.

Tracking—Gas Mixing System: Two gas mixing systems are needed, one for the Station 1 chambers with CF_4 -isobutane and one for the Station 2, 3 and 4 chambers using Ar -ethane. These systems are based on MKS mass flow controllers and the MKS 647 multichannel gas flow and pressure controller. Each system will cost approximately \$12,500.

Data Acquisition: A system consisting of two VME crates with processors/networks adaptors being considered.

Table 7: The multipliers for escalation rate assumptions for construction and information technology (IT) projects.

| Fiscal | | | Fiscal | | |
|--------|---------|-------|--------|---------|-------|
| Year | Constr. | IT | Year | Constr. | IT |
| 2003 | 1.021 | 1.008 | 2006 | 1.106 | 1.032 |
| 2004 | 1.046 | 1.017 | 2007 | 1.135 | 1.041 |
| 2005 | 1.076 | 1.022 | | | |

Table 8: The institutional overhead charged to by collaborating institutes

| Institute | | rate |
|--------------------------------|-----------------------------|-------|
| Abilene Christian University | Capital Equipment | 0% |
| Argonne National Laboratory | Purchase Requests | 10% |
| | Other Direct Costs (Effort) | 26.4% |
| Los Alamos National Laboratory | Capital Equipment | 0% |
| Texas A&M University | Capital Equipment | 0% |

Counting House Computing: Computing requirements for the experimental counting house include a tape copying station (\$5,000), two work stations (\$2,500 each) and a RAID disk system/workstation (\$5,000). These systems will run the Linux OS.

The all costs given here include contingency and, escalation, and institutional overhead. The included contingency varies from 15% to 25% depending on the design stage of each project and has been discussed with the individual detector elements. The escalation rates were taken from “Escalation Rate Assumptions for DOE Projects (as of January 2002)” and is reproduced as Tab. 7. Finally, the institutional overhead is shown in Tab. 8.

5 Collaboration

The core of the collaboration, Abilene Christian University, Argonne National Laboratory, Fermilab, Los Alamos National Laboratory, Texas A&M University and Valparaiso University has recently successfully completed the E866 Drell-Yan experiment at Fermilab. These groups encompass the key technologies needed for the new measurements. The Rutgers group has experience in high rate drift chamber systems. In addition to their E866/NuSea experience, members of the collaboration have been involved in many previous Drell-Yan and muon pair fixed target experiments at Fermilab including E789, E772 and E605.

Argonne will be responsible for the design and construction of the M1 focusing magnet. The primary responsibilities for many of the other elements of the detector will remain as they were in E866. In terms of the money requested in this grant, Texas A&M will be responsible for the design and implementation of the trigger. Los Alamos will be responsible for the station 4 tracking and Abilene Christian will handle the hodoscope arrays. Individual biographical sketches of the primary participants may be found in Appendix 7.

6 Facilities and Resources

The experiment plans to take maximum advantage of already existing facilities and equipment. Much of this equipment has been previously mentioned, but in considering the available resources, it is worth recapping these resources in one coherent place. The tracking chambers and electronics for stations 1, 2 and 3 and the electronics for stations 4 will come from previous experiments (E866/NuSea and E871/HyperCP). The readout for these stations already exist in the Fermilab PREP electronics pool. Roughly 40% of the phototube-base-shield combinations needed for the hodoscopes are being recovered from E866/NuSea. The JGG magnet, as well as all of the power supplies needed for both magnets exist at Fermilab. In addition, major parts of the old SM12 magnet are being “recycled” for use in the new M1 magnet. These parts include the flux return steel, the shelves on which the coils are located and possibly the beam dump. The material in the muon-id wall used by E866/NuSea will be reconfigured by Fermilab for E906. Finally, the liquid hydrogen and deuterium targets from E866/NuSea will be reused.

Fermilab will be providing significant facilities and infrastructure for the experiment. In addition to hosting the experiment and providing the proton beam from the Main Injector, beam line instrumentation, experimental hall and electronics/counting rooms, Fermilab will be providing for the assembly and installation of the M1 magnet and installation remounting of the JGG for this experiment. Fermilab is already providing storage for the E866/NuSea and E871/HyperCP equipment which is going to be reused by E906.

The design work for the new M1 magnet is being done at Argonne by personnel from the ASD division (a part of the Advanced Proton Source). This group has vast experience in designing and realizing magnets for physics experiments. This group includes J.M. Jagger, who along with C.N. Brown of Fermilab (also a member of this collaboration) was responsible for the realization of the SM12 magnet which is being replaced by the new M1 magnet [71].

TAMU–electronics facilities?

ACU–Fermilab scint shop?

LANL?

7 Conclusions

Fermilab E906 will use the 120 GeV primary proton beam from the Main Injector to measure Drell-Yan yields for hydrogen, deuterium and three nuclear targets. These measurements will provide precise new information on:

- the ratio \bar{d}/\bar{u} and the difference $\bar{d} - \bar{u}$ distributions of the proton over the x range of 0.2-0.45 and new insight into the non-perturbative origin of the parton distributions (3.4×10^{18} incident protons),
- the sum $\bar{d} + \bar{u}$ through measurements of the absolute Drell-Yan cross sections,
- the energy loss of colored partons traveling through cold nuclear matter (1.8×10^{18} incident protons), and
- the nuclear dependence of the antiquark distributions over a similar x range.

These measurements should also help resolve nuclear ambiguities inherent in obtaining nucleon antiquark distributions from neutrino data on nuclear targets.

The muon spectrometer needed to carry out this program of measurements is based upon the spectrometers used in previous Fermilab Drell-Yan experiments. Much of the equipment from

this previous experiments will be reused in the reconfigured spectrometer. Some elements of the spectrometer will need to be replaced for the new experiment. The largest cost associated with this replacement is the construction of a new muon focusing magnet at a cost of \$1.96M. New detector, readout, trigger and data acquisition equipment will cost an additional \$720k. The experiment hopes to be able to begin running in January, 2007. In order to meet this deadline, the collaboration requests \$601,000 in FY2005, \$1,560,000 in FY2006 and \$516,000 in FY2007.

Biographical Sketches

References

- [1] H. L. Lai *et al.*, Phys. Rev. D **55**, 1280 (1997).
- [2] H. L. Lai *et al.*, Eur. Phys. J. D **12**, 375 (2000).
- [3] J. Pumplin, *et al.*, J. High Energy Phys. **07** 012 (2002).
- [4] A. D. Martin, R. G. Roberts and W. J. Stirling, Phys. Lett. B **419**, 1280 (1997).
- [5] A. D. Martin, R. G. Roberts, W. J. Sterling and R. S. Thorne, Eur. Phys. J. **C4**, 463 (1998).
- [6] M. Glück, E. Reya, and A. Vogt, Eur. Phys. J. **C5**, 461 (1998).
- [7] P. Amaudruz *et al.*, Phys. Rev. Lett. **66**, 2712 (1991); M. Arneodo *et al.*, Phys. Rev. D **55**, R1 (1994).
- [8] A. Baldit *et al.*, Phys. Lett. B **332**, 244 (1994).
- [9] E. A. Hawker *et al.* (FNAL E866/NuSea Collaboration) Phys. Rev. Lett, **80** 3715 (1998).
- [10] J.-C. Peng *et al.* (FNAL E866/NuSea Collaboration) Phys. Rev. D **58**, 092004 (1998).
- [11] R. S. Towell *et al.* (FNAL E866/NuSea Collaboration) Phys. Rev. D **64**, 052002 (2001).
- [12] D. F. Geesaman, K. Saito and A. W. Thomas, Ann. Rev. Nucl. Part. Sci **45**, 337 (1995).
- [13] FNAL E866/NuSea Collaboration, M.A. Vasiliev *et al.*, Phys. Rev. Lett. **83**, 2304 (1999).
- [14] CKM Collaboration, P.S. Cooper *et al.*, Charged Kaons at the Main Injector: A proposal for a Precision Measurement of the Decay $K^+ \rightarrow \pi^+ \nu \bar{\nu}$ and Other Rare K^+ Processes at Fermilab Using the Main Injector, 2 April 2001.
- [15] A. D. Martin, W. J. Stirling and R. G. Roberts, Phys. Lett. B **252**, 653 (1990).
- [16] R. D. Field and R. P. Feynman, Phys. Rev. D **15**, 2590 (1977).
- [17] D. A. Ross and C. T. Sachrajda, Nucl. Phys. B **149**, 497 (1979).
- [18] F. M. Steffens and A. W. Thomas, Phys. Rev. C **55**, 900 (1997).
- [19] W. Melnitchouk, J. Speth, and A.W. Thomas, Phys. Rev. D **59**, 014033 (1999).
- [20] A. Szczurek *et al.*, Nucl. Phys. A **596**, 397 (1996).
- [21] P.V. Pobylitsa, M.V. Polyakov, K. Goeke, T. Watabe, and C. Weiss, Phys. Rev. D **59**, 034024 (1999).

- [22] A. E. Dorokhov and N. I. Kochelev, Phys. Lett. B **304**, 157 (1993); Phys. Lett. B **259**, 335 (1991).
- [23] P. Geiger and N. Isgur, Phys. Rev. D **55**, 299 (1997).
- [24] S. Kumano, Phys. Rev. D **43**, 3067 (1991); **43**, 59 (1991); S. Kumano and J. T. Londergan, Phys. Rev. D **44**, 717, (1991).
- [25] G. t'Hooft, Phys. Rev. D **14**, 3432 (1976).
- [26] T. Affolder *et al.* (CDF Collaboration), Phys. Rev. D **64** 032001 (2001); Erratum-ibid. D **65** 039903 (2002).
- [27] G. T. Bodwin, Phys. Rev. D **31**, 2616 (1985); **34**, 3932 (1986).
- [28] G. T. Bodwin, S. J. Brodsky and G. P. Lepage, Phys. Rev. D **39**, 3287 (1989).
- [29] W. G. Seligman *et al.*, Phys. Rev. Lett. **79**, 1213 (1997)
- [30] U.K. Yang *et al.* (CCFR/NuTeV Collaboration), Phys. Rev. Lett. **86**, 2742 (2001); and M. Vakili *et al.*, Phys. Rev. D **61** 052003 (2000)..
- [31] K. Akerstaff *et al.* (HERMES Collaboration) Phys. Rev. Lett. **81**, 5519, (1998).
- [32] X. Jiang *et al.* "Measurement of Charge Pion Production Ratios in Semi-Inclusive Deep-Inelastic Scattering at 6GeV", Jefferson Laboratory Proposal PR-02-107 (2002).
- [33] Jefferson Laboratory Hall A Collaboration, "Hall A 12 GeV Upgrade Conceptual Design," 3 October 2002.
- [34] J. Sterling, Letter to John Peoples, May 1998.
- [35] G. Moreno *et al.*, Phys. Rev. D **43**, 2815 (1991).
- [36] P. L. McGaughey *et al.*, Phys. Rev. D **50**, 2038 (1994).
- [37] J. Webb, Ph.D. Thesis, New Mexico State University, (2002).
- [38] W. Melnitchouk and A.W. Thomas, Phys. Lett. B **377** 11 (1996).
- [39] S. Kuhlmann *et al.*, Phys. Lett. B **476**, 291 (2000).
- [40] J.J. Aubert *et al.* (EM Collaboration) Phys. Lett. **123B** 275 (1983).
- [41] D.M. Alde *et al.*, Phys. Rev. Lett. **64**, 2479 (1990).
- [42] J. Carlson, R. Schiavilla, Rev. Mod. Phys. **70** 743 (1998).
- [43] F. Coester private communication; E. T. Berger, F. Coester and R. B. Wiringa, Phys. Rev. D **29** 398 (1984).
- [44] G. E. Brown *et al.*, Nucl. Phys. A **593** 295 (1995).
- [45] H. Jung and G. A. Miller, Phys. Rev. C **41** 659 (1990).
- [46] A. E. L. Diepernik and C. L. Korpa, Phys. Rev. C **55** 2665 (1997).

- [47] K. Adcox *et al.* (PHENIX Collaboration), Phys. Rev. Lett. **88**, 022301 (2002).
- [48] C. Adler *et al.* (STAR Collaboration), nucl-ex/0206011.
- [49] K. Adcox *et al.* (PHENIX Collaboration), nucl-ex/0207009.
- [50] C. Adler *et al.* (STAR Collaboration), nucl-ex/0206006.
- [51] Quark Matter 2002 Conference, Nantes, France, July, 2002. <http://alice-France.in2p3.fr/qm2002/ScientificProgram/program.htm>. See especially presentations by D. D'Enterria (PHENIX, high- p_T π^0), J. Klay (STAR, high- p_T inclusive charged hadrons), J. Jiangyong (PHENIX, high- p_T inclusive charged hadrons), K. Filimonov (STAR, high- p_T elliptic flow), and D. Hardtke (STAR, back-to-back jets in p+p and Au+Au).
- [52] S. Gavin and J. Milana, Phys. Rev. Lett. **68**, 1834 (1992).
- [53] S.J. Brodsky and P. Hoyer, Phys. Lett. B **298**, 165 (1993).
- [54] R. Baier *et al.*, Nucl. Phys. B **484**, 265 (1997); R. Baier *et al.*, Nucl. Phys. B **531**, 403 (1998).
- [55] K.J. Eskola, V.J. Kolhinen and P.V. Ruuskanen, Nucl. Phys. B **535**, 351 (1998); K.J. Eskola, V.J. Kolhinen and C.A. Salgado, Eur. Phys. J. C **9**, 61 (1999).
- [56] M.B. Johnson *et al.*, Phys. Rev. C **65**, 025203 (2002).
- [57] F. Arleo, Phys. Lett. B **532**, 231 (2002).
- [58] E. Wang and X.N. Wang, hep-ph/0202105.
- [59] M. Hirai, S. Kumano, and M. Miyama, Phys. Rev. D **64**, 034003 (2001).
- [60] V. Papavassiliou, Contribution to the Main Injector Stationary Target Workshop, Fermilab, May 1997.
- [61] FNAL E866/NuSea Collaboration, C.N. Brown *et al.*, Phys. Rev. Lett. **86** (2001) 2529; T.H. Chang, Ph.D. Thesis, New Mexico State University, 1999, hep-ex/0012034.
- [62] FNAL E866/NuSea Collaboration, M.J. Leitch *et al.*, Phys. Rev. Lett. **84**, (2000) 3256; W.M. Lee, Ph.D. Thesis, Georgia State University.
- [63] NA3 Collaboration, J. Badier *et al.*, Z. Phys. **C20**, (1983) 101.
- [64] A. Walters, private communication.
- [65] C. A. Gagliardi *et al.*, Nucl. Instrum. Methods A **418**, 322 (1998).
- [66] P906 Collaboration, D.F. Geesaman *et al.*, *Response to PAC Questions on P906 Proposal for Drell-Yan Measurements of Nucleon and Nuclear Structure with the FNAL Main Injector*, 10 June 1999, (unpublished).
- [67] Fermilab Main Injector Technical Design Handbook, 1994, <http://www-fmi.fnal.gov>.
- [68] Y-C Chen, Inst. of Phys., Academia Sinica, private communication.
- [69] Greg Bock, NuMI Project: Project Overview, presented to the DoE Office of Science Review of the NuMI Project, 30 January 2002.

[70] J. M. Jagger and K. M. Thompson, *Cost estimate of P906 magnet*, revised July, 2002.

[71] R.W. Fast *et al.* *14.4 m Large Aperature Analysis Magnet with Aluminum Coils*, Fermilab report TM-1034.